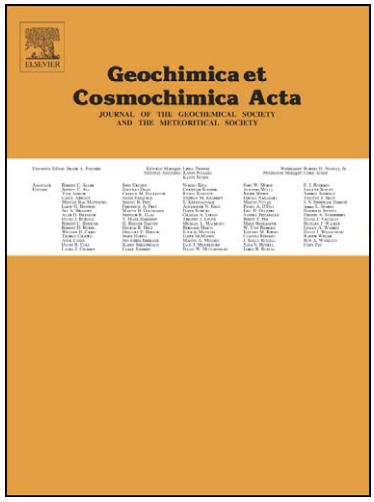

Petrology of the Unbrecciated Eucrites

R.G. Mayne, H.Y. McSween Jr., T.J. McCoy, A. Gale

PII: S0016-7037(08)00656-X
DOI: 10.1016/j.gca.2008.10.035
Reference: GCA 5899

To appear in: *Geochimica et Cosmochimica Acta*

Received Date: 2 August 2007
Accepted Date: 8 October 2008

Please cite this article as: Mayne, R.G., McSween Jr., H.Y., McCoy, T.J., Gale, A., Petrology of the Unbrecciated Eucrites, *Geochimica et Cosmochimica Acta* (2008), doi: 10.1016/j.gca.2008.10.035

Petrology of the Unbrecciated Eucrites

by

R.G. Mayne[1,2], H.Y. McSween Jr.[1], T.J. McCoy[2], and A. Gale[3]

1. Department of Earth and Planetary Sciences, University of Tennessee, Knoxville, TN 37996-1410
2. Smithsonian Institution, National Museum of Natural History, 10th & Constitution NW, Washington, DC 20560-0112
3. Department of Earth and Planetary Sciences, Harvard University, 20 Oxford Street, Cambridge MA 02138

Resubmitted September 8th. 2008.

Abstract

Twenty-nine unbrecciated eucrites have been thoroughly characterized in terms of the petrologic factors that affect their spectra, such as mineral chemistry, modal adundances, grain sizes, and textures. We have conducted a combined petrologic and spectral study designed to provide insight into the petrogenesis of the basaltic crust of Vesta and the variety of rock-types that exist within it, as well as aid in the petrologic interpretation of spectra to be collected by the Dawn orbiting spacecraft. This paper details the petrology part of the study. Unbrecciated eucrite samples were selected to avoid the complications of lithologic mixing in the accompanying spectral study. A wide variety of textural types are seen within the basaltic eucrites, encompassing quenched, coarse-grained, and granoblastic samples. Zoned pyroxenes in eucrites and those that preserve a history of initial rapid cooling are rare. Nearly all eucrite samples have been thermally metamorphosed and would commonly be classified as equilibrated; however, this term reflects only the quadrilateral (Mg, Fe, Ca) compositions of pyroxenes, and considerable variations are seen within the minor elements (Al, Ti, and Cr) in pyroxenes as well as plagioclase compositions. Determination of both pyroxene and plagioclase compositions together with pyroxene geothermometry provides a better estimate for the relative degree of thermal metamorphism a eucrite has experienced. The petrologic differences observed here might allow different eucrites to be distinguished spectrally. This is especially true for the varying pyroxene compositions as the spectra of eucrites are dominated by absorption features attributed to pyroxene.

1. Introduction

The HED meteorites include the basaltic and cumulate eucrites (basalts and gabbros, respectively), diogenites (orthopyroxenites), and howardites (breccias composed primarily of eucrites and diogenites), which together constitute the largest group of achondrites. These meteorites are linked by oxygen isotope compositions that define a common mass fractionation line (Clayton and Mayeda, 1996), and their radiometric ages indicate asteroid differentiation and magmatism within ~10 million years of the formation of the solar system (Wadhwa et al., 2006). They are commonly believed to have originated on 4 Vesta (McCord, 1970; Consolmagno and Drake, 1977; Drake, 2001; Keil, 2002), a large differentiated asteroid in the main belt. Vesta itself is of great interest, as it appears to represent one of the few protoplanets that have survived intact since their formation early in solar system history (e.g. Drake, 2001). Several competing models for Vesta's differentiation have been proposed (e.g. Mason, 1962; Stolper 1977; Righter and Drake, 1997; Ruzicka et al., 1997), but none has been able to explain all aspects of the inferred geologic evolution of Vesta and reproduce the complex geochemical relationships seen within the entire suite of HED rocks (Mittlefehldt and Lindstrom, 2003).

The Dawn mission, which launched September 2007, will carry, among other instruments, a mapping spectrometer, VIR (Visible Infrared), which will provide measurements in the visible near-infrared (VIS-NIR) range: 0.25μm – 5μm (Russell et al., 2006). This instrument will analyze the surface of Vesta from orbit and enable the production of surface spectral maps (Russell et al., 2002). In order to interpret such maps

it is important that the HEDs themselves are well characterized petrologically, and that the mineralogical and textural factors that affect their spectra are well understood and quantified. We expect that linked petrology and spectra may then allow us to establish a geologic context for the HEDs, the properties of which suggest formation as surface flows, plutons within the deeper crust, and regolith materials.

Gaffey (1997) observed sub-hemispheric color and spectral variations across the surface of Vesta as it rotated, corresponding to regions with differing mineralogies. He produced a generalized lithologic map of Vesta, describing surface units as eucrite-rich or diogenite-rich. Binzel et al. (1997) utilized Hubble Space Telescope images to compile their own geologic map of Vesta. They observed contrasts in albedo and composition between the western and eastern hemispheres, which suggest a difference in rock types. A predominantly basaltic mineralogy, analogous to eucrites, was suggested for the western hemisphere, whereas the east appeared to show a plutonic (diogenetic) component. They suggested that a major impact event might have preferentially excavated plutonic material in the eastern hemisphere. With a resolution of 170-615 m/pixel, depending on the planetocentric radius of the orbit (Russell et al., 2006), Dawn's VIR will vastly improve our knowledge of the spectral variability on the surface of Vesta, and therefore allow the lithologic differences and distributions of units to be investigated.

This paper focuses on the petrology of the unbrecciated eucrites, and is part of a larger study exploring the link between the petrologic and spectral characteristics of these samples. Approximately 85% of the eucrites are polymict or monomict breccias, and most of the eucrite literature has focused on breccias (e.g. Delaney et al., 1984a; Hsu and Crozaz, 1996; Kitts and Lodders, 1998; Mittlefehldt and Lindstrom, 2003) rather than the

less common unbrecciated meteorites. If we are to understand exactly what factors influence the spectra of the eucrites, the unbrecciated samples are the key as they avoid the complications of lithologic mixing. Here we define unbrecciated eucrites as those that currently show no evidence for brecciation. This definition may potentially include some eucrites that are thoroughly recrystallized breccias (e.g. Yamaguchi et al., 1996; 1997c). Unbrecciated eucrites also provide valuable insight into a variety of eucrite rock-types, reflecting the lithologic heterogeneity that exists within the basaltic crust of Vesta, both at the surface and at depth. If we better understand the relationships between these samples and how they form, we can critically analyze models proposed for their formation and suggest what lithologies may be observed on the surface of Vesta with Dawn.

2. Background

2.1 Eucrite Spectra

In the VIS-NIR wavelength range the spectra of the eucrites are dominated by the pyroxenes they contain. They produce two dominant absorptions at around 1 and 2 μm (Gaffey, 1976). The positions of these two absorption bands are directly proportional to the cations in the octahedral sites, primarily Ca^{2+}, Mg^{2+}, and Fe^{2+} (Adams, 1974; Burns, 1993). The 1 and 2-μm band centers both shift to longer wavelengths as the calcium content of the pyroxene is increased (Adams, 1974; Cloutis and Gaffey, 1991). However, it is the presence of iron (Fe^{2+}) in the pyroxene structure that actually causes the major absorptions. Therefore, in order for us to be able to predict the mineral chemistry of the surface of Vesta with remotely sensed data, we must have not only a knowledge of the

mineral chemistries of the surface rocks, but also an understanding of the influence of these compositions upon the spectra,

The eucrites contain small amounts of ilmenite, chromite, troilite, and native iron-nickel metal. The low albedo in some meteorite spectra is associated with the presence of such opaque phases (Johnson and Fanale, 1973), as they are often dark and spectrally featureless (Cloutis et al, 1990a; 1990b), and act to suppress to the major Fe^{2+} silicate absorption bands (Miyamoto et al., 1981). This characteristic will depend on the type and abundance of the phase present and therefore we attempt to quantify all these factors in order to assess its effect upon the spectra.

Grain size is also known to affect the VIS-NIR spectrum of a sample (e.g. Adams and Filice 1967). The unbrecciated eucrites have grain sizes that vary widely. Serra de Magé is the coarsest grained sample with some grains over a millimeter in diameter, and ALH A81001, the finest grained sample, has a grain size <50 μm. Textural information on all of the unbrecciated eucrites studied is presented here, which includes qualitative information on relative grain size. Quantitative grain-size analysis, using crystal size distribution (CSD) will be presented in a later paper..

2.2 Eucrite Classification

Several existing schemes are used to subdivide the eucrites. Eucrites have been distinguished petrographically and chemically as cumulate and non-cumulate/basaltic rocks (e.g. Consolmagno and Drake, 1977; Stolper, 1977, BVSP, 1981). The basaltic eucrites are then commonly split into two main groups, Stannern and Main-Group-Nuevo Laredo, based on their geochemistry. The difference between these two groups is defined primarily by their incompatible element concentrations and Mg# (Mg/(Mg+Fe)).

The Main Group - Nuevo Laredo trend shows a decrease in Mg# with increasing incompatible element content, whereas the members of the Stannern trend have an almost constant Mg# and overall higher abundances of incompatibles (Stolper, 1977). However, in this study the aim is to petrologically characterize the unbrecciated eucrites and, later, apply this knowledge to better understand their spectra. The geochemical classification into the Stannern and Main Group-Nuevo Laredo trends is not likely to be spectrally significant when compared to factors such as pyroxene mineral chemistry, which is far more likely to affect the resulting reflectance spectrum. Therefore, the prevalent cumulate and non-cumulate/basaltic classification was used here, because they differ texturally and in terms of mineral chemistry, with cumulates having pyroxenes with higher-Mg contents (Consolmagno and Drake, 1977, Stolper, 1977). However, it should be noted that the unbrecciated basaltic eucrites exhibit a much wider range of textures than the cumulates.

3. Analytical Techniques

3.1 Sample Selection

All previously identified unbrecciated eucrites in the meteorite collection at the U.S. National Museum of Natural History (Smithsonian Institution) were examined in thin section, as well as those samples that were not classified in terms of their brecciation state. In general, the non-Antarctic eucrites have been studied in greater detail than the majority of those in the U.S. Antarctic collection. However, we observed that most of the textural variety within the unbrecciated eucrites is seen among meteorites of the Antarctic collection (Mayne et al., 2006). Although we were able to examine more unbrecciated

eucrites from the Antarctic collection than the non-Antarctic (approximately 3:1), this cannot be the sole reason attributed to the difference in textural diversity. Non-Antarctic unbrecciated eucrites are dominated by coarse-grained cumulate samples, whereas Antarctic specimens cover a wide spectrum of textural types. Hand samples of the lesser-studied Antarctic meteorites were also examined at NASA Johnson Space Center, to ensure that thin sections were representative of the samples and to check for brecciation on a larger scale.

It was not possible within the confines of this study to survey all known eucrites; however, we do believe the eucrites chosen here encompass the range of properties seen in this meteorite group. Initially, 29 unbrecciated eucrites (Table 1) were chosen by eliminating meteorite pairs and meteorites known to be breccias. ALH A81001 is an extremely fine-grained, quenched sample and was initially described as polymict (Grossman, 1994); ALH A81313, the only unbrecciated eucrite examined that contains maskelynite, was also classified as a polymict eucrite (Grossman, 1994). Subsequent studies have suggested that ALH A81001 should be reclassified as unbrecciated (e.g. Warren et al, 1996; Mittlefehldt and Lindstrom, 2003). These two eucrites were included because no evidence for brecciation was observed in hand sample or thin section in this study.

Ibitira has been suggested to originate from a different parent body from the majority of the eucrites (Mittlefehldt, 2005), due to its unique oxygen isotope characteristics (Wiechert et al., 2004) and different pyroxene Fe/Mn ratio (Mittelfehldt, 2005). Because of its prominence in the literature it was decided to include Ibitira in this

study. We investigate whether the mineralogic differences between it and the other eucrites are overstated.

3.2 SEM Mapping

Elemental X-ray maps were collected on one thin-section of each of the 29 unbrecciated eucrites using the JEOL JSM-840 scanning electron microscope (SEM) in the Mineral Sciences Department of the Smithsonian Institution. A range of magnifications were used for the samples (Table 1), as it is important to be able to resolve the features within each section while still maintaining a reasonable data collection time. Factors such as grain size and pyroxene exsolution were taken into account in determining resolution; coarser-grained samples were mapped using magnifications as low as 30X, whereas Ibitira, with its fine-scale exsolution, was mapped at 100X. The elemental X-ray maps of Fe, Si, and Al were chosen to create mineral maps of each eucrite thin section studied as, when combined, they are able to delineate the main mineral groups within the eucrites: pyroxene, plagioclase, silica, and the opaque minerals (oxides, sulfides, and metal). Each thin-section was mapped in entirety, or as close to entirety as was possible while maintaining a reasonable collection time.

Each elemental X-ray map consisted of overlapping tiles, which were compiled using image-processing software to produce a mosaic of the area mapped. The selected elemental mosaics (Fe, Si, and Al) were then combined to produce a map of each section, where each mineral phase was denoted by different colored pixels. The relative contributions of each mineral, i.e. the number of pixels of a certain color, were then used to measure the modal abundances for pyroxene, plagioclase, silica, and the opaque minerals. Areas where no mineral phase existed (i.e. pocks or cracks in the section) are

indicated by white pixels and are, therefore, not included in the mode calculation. Modes were calculated three times for each sample map to allow for any color variations using digital pixel counting. The average mode for each sample and the standard deviation calculated for each mineral group are given in Table 2. The standard deviation given (1σ) is derived from the difference between the three different modal calculations. Quantifying the error associated with the compilation of the element mosaics and mineral maps is difficult; however, previous authors have suggested it can largely be attributed to the difficulty of determining phase boundaries, given the limited resolution of the X-ray maps used (Floss et al., 2007).

3.3 Electron Microprobe

Chemical analyses of all major minerals (pyroxene, plagioclase, chromite, ilmenite, sulfides, metal) except silica (SiO_2) were made using the Cameca SX-50 electron microprobe at the University of Tennessee. Analytical conditions were: 15 kV, 20 or 30 nA, 1-μm beam for pyroxene, chromite, ilmenite, and metal; 15 kV, 20 nA, 5-μm beam for plagioclase and sulfides. ALH A81001 contained a silica-enriched plagioclase glass and this was analyzed at 15kV, 10nA, 1-μm beam. Counting times were 20 sec for each element, apart from Zr, which was 60 sec. A correction was applied to the spinel analyses that contained vanadium, due to interference between the TiKβ and VKα peaks (Snetsinger et al., 1968). Tables 3-7 present representative analyses for each major mineral phase present in the sections studied. Previous studies of eucrites have reported the presence of tridymite (e.g. Delaney et al., 1984a; Yamaguchi et al., 2001), cristobalite (e.g. Yamaguchi and Mikouchi, 2005; Chennaoui Aoudjehane and Jambon, 2007), and quartz (Treiman et al., 2004). However, in this study, we did not determine

the mineralogy of the silica phase. Fe_2O_3 concentrations were not calculated for pyroxene or oxide minerals in these samples, as previous bulk chemical analyses reported by Jarosewich (1990) did not find the presence of ferric iron in any HED meteorite. All reported analyses have good oxide totals (>98%) and stoichiometry. All errors reported for elemental compositions or ratios are given as 2σ, and are calculated from the counting errors associated with the analytical conditions used. All ternary diagrams in this paper were plotted using the freeware program Δplot (John, 2004).

4. Results

4.1 Textural Variations

All the mineral maps not used as figures within this paper are given in the electronic annex. Each map delineates plagioclase, pyroxenes, silica and opaque phases (chromite, ilmenite, troilite, kamacite, and taenite). These maps do not allow different pyroxene compositions to be distinguished, so both high- and low-Ca pyroxene are grouped together. Higher resolution maps allowing the differentiation between high- and low-Ca pyroxenes were collected only for those samples that will be included in the later spectral part of this study. Examples of the mineral maps, which cover the range of textures observed, are shown in Figure 1.

4.1.1 Basaltic Eucrite Textures

QUE 94484 is the only coarse-grained eucrite to contain elongate radiating plagioclase grains that in some areas reach over a millimeter in length. QUE 94484 (Figure 1a) contains abundant interstitial areas that are rich in silica and troilite, relative

to other samples. These areas appear to be late-stage and probably represent residual melt pockets (*Antarctic Meteorite Newsletter 19-1*).

ALH A81001 (Figure 1b) is the finest-grained sample studied, with most grains being no larger than 200 µm. In some previous studies it has been identified as a possible impact melt (e.g. Delaney et al., 1984b). It has a vitrophyric texture and the "plagioclase" illustrated in Figure 1b is, in fact, glass having the composition of plagioclase plus silica. Pyroxene grains are lath-like, skeletal and often radiating (Figure 2a). Pyroxene phenocrysts reaching up to half a millimeter in size are found within this meteorite, although they are uncommon (Figure 2b) and probably crystallized before eruption. The map of ALH A81001 shows fine-grained areas with pyroxene grains typically between 50 and 100 µm. These domains superficially resemble clasts, explaining its original polymict classification (Grossman, 1994). On closer microscopic inspection, however, pyroxene grains can be seen spanning the 'boundaries' between areas of different grain sizes, so the apparent clast relationship is an artifact and the sample can be described as texturally heterogeneous but unbrecciated. Fine-grained ilmenite is scattered throughout (Figure 2c), but it is not visible on the mineral map due to its small grain size (down to sub-micron in some grains) and it does not represent a significant modal component. Other fine-grained eucrites contain opaque phases (chromite, ilmenite, troilite, and kamacite) and silica on a scale that can be seen using the SEM mapping technique.

Coarser grained basalts are prevalent within the eucrites. Most of these samples exhibit a subophitic to ophitic texture (Table 1). Shock effects are relatively common and often cause granulation or fracturing of the samples. Chervony Kut (Figure 1c), a

coarse-grained non-cumulate eucrite, retains its original igneous texture (sub-ophitic) despite being cataclasticized (Figure 2d). Previous authors have suggested that its origin can be attributed to comparatively slow magmatic crystallization followed by cataclasis and minor subsolidus recrystallization (Gooding et al., 1979). The unbrecciated eucrites show a range of features caused by shock metamorphism on their parent body. These range from fracturing, as described for Chervony Kut above, to mosaicism of grains. For example, MAC 02522 has mosaicized pyroxene. A few samples eucrites contain shock-melted veins, such as LEW 85353 and EET 90029.

4.1.2 Granoblastic Textured Basaltic Eucrites

Five of the unbrecciated eucrites in this study have not completely preserved their original igneous textures. However, a range of metamorphic overprints is observed, from Ibitira (Figure 1d), which exhibits an entirely granoblastic, fine-grained texture (Steele and Smith, 1976; Mittlefehldt, 2005), to BTN 00300 in which remnants of the original sub-ophitic texture remain (Mittlefehldt and Galindo, 2002). Both LEW 85305 and EET 90020 contain inequigranular granoblastic textures.

Ibitira also contains vesicles, which are an unusual feature in extraterrestrial basalts (McCoy et al., 2006). For terrestrial basalts that contain vesicles, the assumption is that they represent surface lava flows with CO, CO_2, or H_2O as the vesicle-forming gases (Wilkening and Anders, 1975); however, surface formation cannot necessarily be evoked for the vesicular eucrites. McCoy et al. (2006) concluded that vesicular basalts on asteroids require formation at depth. The lack of an atmosphere on these bodies means that there is no limit on the expansion of gas, so gas escape processes would be

very efficient. Because of this unusual formation mechanism, in dikes at depth, vesicular eucrites may be a relatively uncommon occurrence.

One very interesting feature of this group is that only the samples with a granoblastic texture contain tabular silica grains. GRA 98098 (Figure 1e) is a relatively coarse-grained, texturally distinctive sample. Elongate white veins of silica can be seen in hand sample (Mittlefehldt and Lee, 2001). They appear to be a late-crystallizing phase as they overgrow or enclose the grains around them. In the section studied here, one lone silica grain is seen to cut across the entire thin section, so no conclusions can be made as to its overall length (Figure 1e). Smaller millimeter-sized tabular silica grains are found in Ibitira (Figure 1d). BTN 00300 also contains a few small tabular silica grains that crosscut the surrounding mineralogy, but not all the silica in the sample shows the same morphology. LEW 85305 contains an area in the section where silica is abundant and poikilitcally encloses the minerals around it, suggestive of a large silica grain such as that in GRA 98098. However, it is harder to establish if this feature is one continuous grain.

4.1.3 Cumulate Eucrite Textures

Serra de Magé (Figure 1f) is one of the coarsest grained samples in this study, with pyroxene grains up to half a centimeter in size, whereas Moama has a much smaller grain size of under a millimeter. These samples show the coarsest exsolution lamellae of all the unbrecciated eucrites, as would be expected due to their slow cooling rate.

4.2 Modal Mineralogy

The unbrecciated eucrites are predominantly pyroxene-plagioclase basalts (Table 2), with lesser amounts of silica, ilmenite, chromite, troilite, and metal (kamacite in all but one sample) and rare late-stage phases such as fayalitic olivine, baddeleyite, and

phosphates. Figure 3 illustrates the measured variation in pyroxene and plagioclase abundances and modal abundances for all the unbrecciated eucrites, as given in Table 2. The majority of samples have <1 vol.% opaque minerals (oxides, troilite, and metal). The amount of silica in most thin sections is also low; however, this is much more variable with percentages ranging from 0 to <13 vol.%. GRA 98098 has a relatively high modal percentage of silica (8 vol.%) due to the one large grain that crosscuts the section. QUE 94484 and ALH A8100 have distinctive modal mineralogy: QUE 94484 has abundant late-stage phases relative to other samples (>2 vol.% opaque phases and >7 vol.% silica), and ALH A81001 contains no modally significant minor phases at all and has the lowest pyroxene to plagioclase ratio (Figure 3). Ilmenite is present (Figure 2c) in this sample but, as previously discussed, it is so fine grained that it is not shown on the SEM maps.

4.3 Mineral Chemistry

4.3.1 Pyroxenes

Compositional data for pyroxenes in all 29 unbrecciated eucrites are shown in Figure 4. It can be observed that orthopyroxene, pigeonite, and augite all occur within these samples.

The quadrilateral pyroxene compositions of all of the unbrecciated eucrites can be discussed in terms of the classification of Takeda and Graham (1991), who defined three main chemical zoning trends within the eucrite group (Figure 5 a-c). The majority of the unbrecciated eucrites in this study follow the Fe-Ca trend (Figure 5c), representing the variation from host pigeonite to exsolved augite in what have been called “ordinary” or equilibrated (Reid and Barnard, 1979) eucrites. QUE 94484, MAC 02522 (the zoned-pyroxene basalts) and, to a lesser extent, PCA 97053 (all shown in Figure 4) follow the

Mg-Fe-Ca trend of Pun and Papike (1996), shown in Figure 5a. QUE 94484 pyroxenes show the most extensive zoning out of all the unbrecciated eucrites. Its pyroxenes contain low-Ca, Mg-rich cores and trend towards more Fe-rich, low-Ca compositions towards the rim and continue through increasing Ca contents. MAC 02522 pyroxenes, have one fairly uniform pyroxene composition and appear to have experienced Fe-Mg diffusion, suggesting partial equilibration, but they have not exsolved into two separate pyroxene compositions. PCA 97053 appears almost entirely equilibrated, with a few analyses indicating that some zonation may remain.

The cumulate eucrites can all be distinguished as they have more En-rich compositions. It was noted in the original classification of ALH A81313 that there appeared to be pyroxene- and plagioclase-rich layers present, suggesting a possible cumulate origin (*Antarctic Meteorite Newsletter* 8-1). We have grouped it here with the other cumulate eucrites and the quadrilateral pyroxene compositions would seem to support this, as ALH A81313 has compositions that match those of the cumulates, especially Serra de Magé (Figure 4). This sample should probably be reclassified as a cumulate eucrite.

ALH A81001 contains two populations of pyroxenes. It is the only sample that contains pyroxene phenocrysts, which are assumed to have formed before the magma reached the surface. These phenocrysts have a composition that is significantly lower in Ca than that of the rest of the sample, having Wo contents between 1 and 2%, compared to >20%. They do not represent a significant modal component but do appear to have compositions that are related to the primary pyroxene in the sample, as they plot on an extension of the tie line defined by non-phenocrysts in the pyroxene quadrilateral.

Plots of the minor elements Al, Cr, and Ti in pyroxenes were also constructed (smaller inset ternary plots in Figure 4). Despite most of the unbrecciated eucrites qualifying as equilibrated in terms of their quadrilateral components, a great diversity of compositions is observed among these minor elements. Some appear clustered (and therefore well equilibrated themselves), but most others show two trends (Figure 4). Trend 1 reflects a relatively constant Ti content with variation in Cr and Al contents (the most prevalent trend), and trend 2 shows a relatively constant Cr content with variation in Ti and Al contents. There are some samples, like LEW 88010, that appear to contain ppyroxenes showing both trends. Chervony Kut demonstrates trend 1 well and, although it is seen in a number of other samples, it is not always as clearly defined. Trend 2 is less common among the unbrecciated eucrites, with LEW 85353 providing the best example. The possibility that these trends corresponded to a mixing line between high and low-Ca pyroxenes (exsolution) was examined, but there appears to be no link between Ca content and minor element composition.

Pun and Papike (1996) discussed the expected crystallization sequence for the eucrites, in terms of pyroxene substitution couples. Basaltic assemblages begin at Cr-rich compositions, becoming more Al-rich as Cr is removed from the melt. This would involve both the $^{VI}Cr^{3+}$-$^{IV}Al^{3+}$ and $^{VI}Al^{3+}$-$^{IV}Al^{3+}$ couples, gradually shifting to the $^{VI}Al^{3+}$-$^{IV}Al^{3+}$ couple as Cr is depleted. When plagioclase starts to crystallize the pyroxene is competing for Al, resulting in a shift to the $^{VI}Ti^{3+}$-$^{IV}Al^{3+}$couple. The unbrecciated eucrites in this study that have not been equilibrated with respect to their minor element compositions appear to follow such a sequence. Trend 1 reflects early pyroxene crystallization before the onset of plagioclase, with little variation in Ti content, while

trend 2 represents those pyroxenes crystallizing after plagioclase reached the solidus. Those unbrecciated eucrites that contain minor-element pyroxene compositions showing both trends represent pyroxenes in that crystallized continuously before and after plagioclase crystallization began.

Fe/Mn ratios in pyroxenes are thought to be a diagnostic tool for determining if samples have a common planetary origin (Papike et al., 2003), as the primordial values of these elements are believed to remain constant throughout planetary differentiation (Papike, 1998). Oxygen isotopes are also commonly used to distinguish meteorites from different parent bodies. Wiechert et al. (2004) identified four eucrites (Pasamonte, Caldera, ALH A78132, and Ibitira) whose oxygen isotopic compositions deviated from those of the other eucrites. Mittlefehldt (2005) and Lentz et al. (2007) have investigated the possibility that samples with anomalous O isotope values also show distinct pyroxene Fe/Mn ratios. Mittlefehldt (2005) found Ibitira's pyroxene Fe/Mn ratio differed from other eucrites, supporting its derivation from a different parent body. However, Pasamonte and Caldera appear indistinguishable from the general eucrite trend (Lentz et al., 2007). The Fe and Mn data for all pyroxenes in this study were plotted against Fe/Mg and Wo content and examined for distinct values (Figs. 6a and b).

The 29 unbrecciated eucrites define a much broader range of pyroxene Fe/Mn values than have previously been reported; values under 20 and up to almost 45 are measured (Figs. 6a and b). Ibitira pyroxene Fe/Mn ratios are the highest measured, but they overlap the rest of the Fe/Mn pyroxene analyses. This diagram appears to allow cumulate and non-cumulate samples to be distinguished. Pyroxenes in each cumulate sample define a narrow range of Fe/Mg and Wo values but a large range in Fe/Mn,

producing nearly vertical trends in Figure 6a and 6b. The narrow range of Fe/Mg values appears fairly diagnostic of the cumulate group. EET 92023 also demonstrates this pattern with just slightly more scatter in the data, although its origins are debated (see below). However, EET 87520, proposed as a partial cumulate (Mittlefehldt and Lindstrom, 2003), does not mirror the narrow Fe/Mg range seen in the cumulate eucrites. Of all the non-cumulate eucrites studied, QUE 94484 can be distinguished most easily; it has anomalously low pyroxene Fe/Mn ratios.

4.3.2 Plagioclase

The range of plagioclase compositions, expressed as the An (Anorthite $CaAl_2Si_2O_8$) end-member, measured for all samples is shown in Figure 7. No sample has an Or (Orthoclase $KAlSi_3O_8$) content greater than Or_5, and most commonly there is no detectable Or component. The Or contents of analyzed feldspars (plotted as K in atomic formula units against An#) are compared in Figure 8a to the known trends for Moon/Vesta, Earth, and Mars (Papike, 1998; Papike et al., 2003). Most unbrecciated eucrite plagioclase compositions fall close to the previously defined Moon/Vesta line, although they appear to cluster slightly below it. ALH A81001 is excluded from Figures 7 and 8, as this sample actually contains a silica-enriched plagioclase composition glass rather than crystalline plagioclase. The overall range of An_{73-96} compares well with previously reported ranges by Delaney et al. (1984a) and Mittlefehldt et al. (1998), which were An_{65-94} and An_{75-93} respectively. Mittelfehldt (2005) reported that Ibitira had an unusually calcic composition when compared to other basaltic eucrites; however, in this study we found four other unbrecciated eucrites that have plagioclase compositions at, or above, An_{95}, suggesting that such feldspars are not as rare as previously thought. Of the

29 eucrites analyzed, over half appeared to contain zoned plagioclase, with grains typically becoming more An-poor from core to rim. Chervony Kut shows the most unequilibrated plagioclase of any of the unbrecciated eucrites, with some grains ranging from Ab_{91} at the core to Ab_{76} at the rim.

Figure 8b shows the measured range of Fe content within the eucrite plagioclase. The majority of the unbrecciated eucrites have Fe concentrations in their plagioclase that fall within the previous range defined by Papike (1998) of less than 0.06 afu Fe (Figure 8b). There are some samples that lie above this limit, e.g. Caldera, PCA 91078 and QUE 94484. The cumulate eucrites have relatively calcic plagioclase (An>90) and low Fe contents.

4.3.3 Oxides

The unbrecciated eucrites commonly contain ilmenite, ulvöspinel, chromite, troilite, and native-iron metal (Table 8). The chromites have varying compositions, ranging to more titaniferous chromites/ulvöspinel; however, they do not span the whole range of the ulvöspinel-chromite solid solution series (Figure 9a-c). Figure 9c provides a comparison of all these spinels with the work of Yamaguchi (2000), who analyzed the spinels of eucrites with different metamorphic histories. Most unbrecciated eucrites fall within the range of highly metamorphosed eucrites (type 4-6) and, viewed as a group, they contain compositions slightly poorer in Ti than those measured by Yamaguchi (2000). There are six samples whose compositions appear to lie partly in the field defined for types 1-2; these are LEW 88009, LEW 88010, PCA 97014, QUE 99658, PCA 91078, and MAC 02522. QUE 94484 does contain spinel minerals; however, this sample

has undergone quite heavy terrestrial weathering and because of this the opaque phases are oxidized, so that we were unable to obtain good analyses.

Many of the basaltic unbrecciated eucrites show a range of chromite/ulvöspinel compositions within one sample. MAC 02522 has the widest range of all the unbrecciated eucrites analyzed. Spinels in the cumulate eucrites, as a group, vary in composition, but within each individual meteorite they are relatively constant. The granoblastic/highly-metamorphosed samples are richer in Cr than all other samples except MAC 02522, which shows a similar enrichment.

Ibitira, like the other granoblastic samples, shows relatively Ti-rich spinels; however, it also contains some spinels that compositionally lie between ulvöspinel and ilmenite, indicating more extreme Ti-enrichment. Annealing experiments (Arai et al., 1998) indicate the TiO_2 content of eucrite spinels increases at high temperature. It has already been observed that Ibitira has a metamorphic texture and, therefore, presumably was exposed to high temperatures, driving the spinel to more Ti-rich compositions. Yamaguchi et al. (1997a; 2000) previously concluded that the extreme Ti-enrichment seen in Ibitira spinels might be related to its complicated thermal history.

Ilmenite is a common minor phase in the unbrecciated eucrites (Table 8). Its composition varies both within and between samples. MgO contents range from 0.3 to over 5.2 wt. %, Cr_2O_3 from 0 to 5.5 wt. %, MnO from 0.59 to 1.5 wt. %, and ZrO_2 from 0 to 0.15 wt %. Rare Zr-rich grains were observed in association with spinels, usually within ilmenite, in a few samples. These grains were too small for accurate wavelength-dispersive electron microprobe analysis; however, a few were observed using energy-dispersive analysis and had a baddeleyite composition.

4.3.4 Troilite, Metal and Mesostasis

Eucrites commonly contain minor amounts of small metal grains, believed to form either during magmatic crystallization at low oxygen fugacity, or during later thermal metamorphism (Duke, 1965). As all the eucrites studied here are unbrecciated and none are believed to be impact melts, the metal they contain must be indigenous to the sample. The native-Fe metal is kamacite with very low Ni and Co contents (<1 wt.% of each in most samples), with the one exception of EET 92023 (see below). Kamacite is most often associated with troilite. The low-Ni metals in the eucrites most likely formed by reduction of FeO in pyroxenes during thermal metamorphism (one of the mechanisms suggested by Duke, 1965). The close association of the metals with silica, which is another product of the breakdown reaction of pyroxene, supports this idea.

EET 92023 metal contains up to 50% Ni, making it the only sample in this study to contain taenite. Ni contents vary from 5 to 39% from core to rim, as also observed by Kaneda and Warren (1998). They also distinguished a compositional discontinuity near the grain edges and suggested that the outer rim, being richer in Ni, may in fact be tetrataenite. They concluded that the FeNi-metal dated from the original igneous crystallization of the rock (Kaneda and Warren, 1998). This compositional difference would seem to support the suggestion that EET 92023 is a clast from a mesosiderite (Mittlefehldt and Lindstrom 1991) and that the metal it contains was not formed by the same mechanism as seen in the rest of the unbrecciated eucrites.

Mesostasis assemblages occur within the unbrecciated eucrites, consisting of predominantly late-stage phases such as silica, olivine, ilmenite, and baddeleyite. Figure

2e shows an area of mesostasis in sample QUE 94484. This sample contains abundant mesostasis, consisting primarily of silica and troilite.

5. Discussion

5.1 Degree of Metamorphic Equilibration

The term 'equilibrated,' when applied to eucrites, refers only to the pyroxene quadrilateral compositions (Pun and Papike 1996). However, the plagioclase compositions measured in so-called equilibrated eucrites are not consistent with this description, as some grains show significant zoning. For example, Chervony Kut plagioclase has an An content that varies by nearly 20 mole% (An_{75-94}), even though its pyroxenes are equilibrated. O'Neill and Delaney (1982) noted that plagioclase in eucrites was more resistant to thermal metamorphism than pyroxene due to the slow Si-Al diffusion kinetics in the coupled albite-anorthite substitution in plagioclase compared the kinetics of Fe-Mg diffusion in pyroxenes. As previously mentioned, the minor elements (Al, Ti, and Cr) in pyroxene (Figure 4) also show considerable variability, despite equilibration of the major elements. It may, therefore, be possible to obtain a more quantitative indicator of equilibration by considering both the major and minor elements of pyroxene as well as zoning within plagioclase. Table 9 compares the equilibration states of these three components. The table is ordered with respect to temperature, calculated for each sample using the QUILF two-pyroxene geothermometer (Andersen, 1993). Because these equilibration temperatures were calculated using pyroxene compositions from grains that are exsolved, the resulting output is the subsolidus exsolution temperature and not that of original igneous crystallization. The total column

sums the "yes" values referring to whether pyroxene major elements (quadrilateral), pyroxene minor elements (Al, Cr, Ti), and plagioclase (An#) are equilibrated. As pyroxene equilibration temperature decreases, the overall equilibration of the eucrites does also. The succession shown in Table 9 indicates that the major elements in pyroxene become equilibrated first, followed by plagioclase, and then the minor elements in pyroxene. Taken together, these three equilibration indices thus provide a more sensitive estimate of the relative degree of metamorphism in eucrites.

Takeda and Graham (1991) also conducted a study of the homogenization of eucritic pyroxenes as a guide to their thermal history. They divided eucrites into six types (Type 1 to 6), reflecting increasing degrees of metamorphism, an additional type 7 was then added later by Yamaguchi et al. (1996). They suggested that most eucrites have undergone at least one subsolidus reheating event resulting from impact or lava flows extruded over a primary lava (Takeda and Graham, 1991). The results from this study also suggest widespread thermal metamorphism on Vesta, with most samples showing equilibration in at least the major elements in pyroxene. Most of the unbrecciated eucrites studied here, as previously mentioned, contain equilibrated, metamorphosed pyroxenes and, therefore, correspond to types 4-6 of Takeda and Graham (1991). QUE 94484, MAC 02522, and PCA 97053 to a lesser extent, are the only samples that exhibit less equilibrated compositions. If we re-examine those samples that contained spinel compositions overlapping the field defined by Yamaguchi (2000) for the type 1-2, least metamorphosed eucrites (LEW 88009, LEW 88010, QUE 99658, and MAC 02522), we observe that these samples do lie at the low-temperature end of our equilibration table.

Therefore, it would appear that despite widespread pyroxene equilibration the three indices used here can distinguish eucrites with different thermal histories.

Earlier we noted that tabular silica grains only occur in the granoblastic samples. Yamaguchi et al. (1997a) postulated that these were the result of partial melting at 1000-1100^{0}C. Barrat et al. (2007) observed that EET 90020 and Y-86763, which are both basaltic eucrites believed to have undergone partial melting, lack the mesostasis seen within other, less metamorphosed, basaltic eucrites. They suggest that metamorphism, partial melting, and then extraction of the partial melt from these samples produced these features. None of the granoblastic unbrecciated eucrites were observed to contain mesostasis and all of them have at least some tabular silica grains, indicating that the formation of the silica grains is related to the high degree of metamorphism experienced by these samples. If Barrat et al. (2007) are correct, then silica may have formed from mobilization and crystallization of the remaining partial melt. Tabular silica grains have also been identified in unequilibrated eucrites (Arai et al., 1998; Buchanan et al., 2000). This may suggest that their formation is unrelated to partial melting; however, in the unequilibrated eucrites the tabular silica grains are found within the mesostasis (Arai et al., 1998; Buchanan et al., 2000), which is notably absent in the granoblastic samples. It is possible that the silica grains found within the two groups (equilibrated/granoblastic and unequilibrated) are formed by different processes.

5.2 Understanding the Petrogenesis of the Basaltic Crust of Vesta

The eucrites are the key to understanding the petrogenesis of the basaltic upper crust of Vesta. Simplified cross-sections of Vesta commonly depict a howardite regolith, a eucrite upper crust, a diogenite lower crust or upper mantle, a dunite or harzburgite

lower mantle, and a metal-rich core. Although this is a useful first-order model, each layer and its relationship to others must be fully understood and any model proposed for Vesta's differentiation must be capable of explaining these. In this study we have focused on the mineralogy and mineral chemistry of the unbrecciated eucrites, because these factors will impact the spectra taken by the VIR aboard the Dawn spacecraft. As a result, without geochemical data, we cannot draw any meaningful conclusions as to the origin of the magmas here, but we can glean information on their crystallization histories and environments of formation.

Yamaguchi et al. (1996) suggested that the widespread thermal metamorphism seen within the eucrites indicates that the crust of Vesta formed as a result of serial magmatism. They envisaged lava flows erupting and cooling rapidly at the surface only to be buried by subsequent lava flows, which underwent the same process. The lower units were then reheated by the lava flows above them, leaving only the uppermost flows unmetamorphosed. The period of volcanism was estimated to have lasted only a few Myr, and modeling suggests it produced a crust over 15 km thick (Yamaguchi et al., 1997b). The process of initial rapid cooling at the surface does not explain the formation of the cumulate eucrites, or coarser grained basaltic samples; however, these samples could have intruded into the earlier buried flows as dikes or small magma chambers (Yamaguchi et al., 1997b). As was previously discussed, McCoy et al. (2006) invoked such a mechanism for the formation of those samples that contain vesicles at a depth of around 5 km.

The prevalence of some degree of metamorphic equilibration throughout the unbrecciated eucrites may support the hypothesis of serial magmatism. Although

metamorphism caused by impact heating must have occurred on local scales, it seems unlikely that impacts can account for the near, if not total, global-scale heating event required (Keil et al., 1997). Zoned and rapidly cooled samples such as QUE 94484 and ALH A81001 are rare, suggesting that they were among the last lavas to crystallize on Vesta's surface. The ages of the basaltic eucrites are found to cluster around 4.47-4.48 Gyr (Blichert-Toft et al., 2002; Bogard et al., 2003), and the cumulates are ~100 Myr younger (Blichert-Toft et al., 2002). The close ages of all the basaltic eucrites also indicate that they were produced during a brief, but voluminous period of magmatism.

However, it should be noted that serial magmatism alone might not be sufficient to explain the levels of reequilibration seen in the unbrecciated eucrites. Serial magmatism occurs on Earth today in Hawaii, and most likely occurred on the Moon in the past, but neither Hawaiian nor lunar basalts show the same degree of metamorphic re-equilibration as the eucrites. Zoned pyroxenes are a common feature in basalts from both areas. This suggests that the internal heat of Vesta, driven by the presence of Al^{26} in the early Solar System, may have contributed significantly to the global-scale metamorphism on Vesta. The lava flows on the surface would then have acted as an insulation blanket, keeping the heat in Vesta, causing the eucrites to become metamorphosed, and the elements within pyroxene and plagioclase to equilibrate.

Recent age dating of eucrite zircons also suggests that the serial magmatism theory cannot explain the widespread metamorphism seen within the eucrites. U-Pb and ^{207}Pb-^{206}Pb dating indicates that the eucrites crystallized early in Solar System history, between 7-20 My after CAI formation (Misawa et al., 2005). Relative age dating of zircons using ^{182}Hf yields an age within 6.8 My of metal-silicate differentiation

(Srinivasan et al., 2007). If the ^{182}Hf age date is correct, then the later metamorphic event occurred at least 8.9 My after zircon crystallization (Srinvasan et al., 2007) and could, therefore, not have been as a result of serial magmatism.

Greenwood et al. (2005) examined the oxygen isotopes of the eucrites and proposed that their homogenous nature required near global-scale melting after initial accretion, supporting the formation of a magma-ocean on Vesta. However, when oxygen isotopes are examined in conjunction with the Fe/Mn ratios from pyroxenes within the unbrecciated eucrites they point to a more complex story. Previous authors have identified eucrites that show different Fe/Mn and oxygen isotopes to the majority of the eucrites (Mittlefehldt, 2005; Wiechert et al., 2004), and other eucrites with just different oxygen isotopes (Lentz et al., 2007). It does not appear that Fe/Mn and oxygen isotopes tell a consistent story. In this paper another eucrite, QUE 94484, was shown to exhibit lower Fe/Mn ratios compared to all other unbrecciated samples. If all the eucrites originate from a common parent body, the variations in oxygen isotopes and Fe/Mn ratios suggest widespread heterogeneity.

6. Summary

This paper discusses the petrology of the unbrecciated eucrites as part of a larger study into the relationship between the petrologic and spectral features of these meteorites. The unbrecciated eucrites were used to avoid the spectral complications of lithologic mixing that occurs with breccias. The eucrites are widely believed to originate from the basaltic crust of asteroid Vesta, one of the targets of the Dawn spacecraft

mission, and we can use these samples not only to explore the variety that exists within Vesta's complex crust, but also as a link to geologic context for the mission.

- The mineral chemistries, modal abundances, and textures of 29 unbrecciated eucrites were analyzed. A wide range of textures was observed, particularly in the Antarctic suite, with samples including quenched vitrophyric to coarse-grained basalts, and cumulate samples. This likely reflects only some of the diversity that must exist within the basaltic crust of Vesta and hints at the complexity of the magmatic processes that went into forming the basaltic crust of 4 Vesta. At present we are only able to speculate on the real variety of rock-types that might currently exist on the surface and be seen by Dawn.
- With few exceptions, the unbrecciated eucrites have been thermally metamorphosed. The relative degree of metamorphic equilibration of the unbrecciated eucrites is assessed using pyroxene quadrilateral (Mg, Fe, Ca) compositions, zoning of minor elements in pyroxene (Al, Ti, Cr), and the range of An contents in plagioclase. These mineralogic components appear to have equilibrated at different rates as the eucrites cooled. These indicators of metamorphism correlate with pyroxene exsolution temperatures calculated by QUILF geothermometry.
- The almost ubiquitous metamorphism of the eucrite suite and the close ages of the basaltic eucrites (Blichert-Toft et al., 2002; Bogard et al., 2003) support the idea that they were formed during a time of serial magmatism (Yamaguchi et al., 1996), early in Solar System history. However, recent age dating suggests that the metamorphism that the eucrites experienced occurred much later than the

crystallization of the eucrites, (Srinivasan et al., 2007), which would require a separate heating event.

- The petrologic data collected here focused primarily on those characteristics that are known to be spectrally important, such as mineral chemistry and abundance. Pyroxene is the dominant mineral in the spectra of the eucrites and the position of the two main bands it produces (at 1 and 2 μm) depend on its composition, in particular the Ca-content (Adams, 1974; Cloutis and Gaffey, 1991). It has been shown above that the eucrites show a range in pyroxene compositions and it is likely that these will be reflected in their spectra. Such spectral differences may allow us to distinguish between different eucrites on the surface of Vesta, e.g. basaltic versus cumulate eucrites, and gain some insight into their thermal histories.

Acknowledgments: Samples analyzed in this study were provided by the Smithsonian National Museum of Natural History. We thank Alan Patchen for all assistance with the electron microprobe and Donald Lindsley for advice in using the QUILF program. We greatly appreciate the constructive reviews given by Akira Yamaguchi, Paul Buchanan, and Allan Treiman. This work was supported by a Graduate Fellowship at the Smithsonian to RGM and NASA Cosmochemistry grant NNG06GG36G to HYM.

References Cited

Adams J.B. 1974. Uniqueness of visible and near-infrared diffuse reflectance spectra of pyroxenes and other rock-forming minerals. *J. Geophys. Res.* 79: 4829-4836.

Adams J.B. and Filice A. 1967. Spectral reflectance 0.4 to 2.0 microns of silicate rock powders. *J. Geophys. Res.* 72:5705-5715.

Andersen D.J., Lindsley D.H., and Davidson P.M. 1993. QUILF: a PASCAL program to assess equilibria among Fe-Mg-Ti oxides, pyroxenes, olivine, and quartz. *Comp. Geosci.* 19:1333-1350.

Arai T., Takeda H., Lofgren G., and Miyamoto M. 1998. Metamorphic transformations of opaque minerals in some eucrites. *Ant. Met. Res.* 11:71-91.

Barrat J.A., Yamaguchi A., Greenwood R.C., Bohn M., Cotton J., Benoit M., and Franchi I.A. 2007. The Stannern trend eucrites: Contamination of Main Group eucritic magmas by crustal partial melts. 2007. *Geochim. Cosmochim. Acta* 71:4108-4124.

Barrat J.A., Blichert-Toft J., Gillet PH., and Keller F. 2000. The differentiation of eucrites: The role of in situ crystallization. *Meteorit. Planet. Sci.*. 35:1087-1100.

BVSP Basaltic Volcanism Study Project. 1981. *Basaltic Volcanism of the Terrestrial Planets.* Pergamon Press, Inc., New York., pp. 214-235.

Binzel R.P. and Xu S. 1993. Chips off asteroid 4 Vesta: Evidence for the parent body of basaltic achondrite meteorites. *Science* 260:186-191.

Binzel R.P., Gaffey M.J., Thomas P.T., Zellner B.H., Storrs A.D., and Wells E.N. 1997. Geologic mapping of Vesta from 1994 Hubble Space Telescope images. *Icarus* 28:95-103.

Blichert-Toft J., Boyet M., Télouk P., and Albaréde F. 2002. ^{147}Sm-^{143}Nd and ^{176}Lu-^{176}Hf in eucrites and the differentiation of the HED parent body. *Earth Planet. Sci. Lett.* 204:167-181.

Bogard D.D., and Garrison D.H. 2003. ^{39}Ar-^{40}Ar ages of eucrites and thermal history of asteroid 4 Vesta. *Meteorit. Planet. Sci.* 38:669-710.

Bowman L.E., Papike J.J., and Spilde M.N. 1999. Diogenites as asteroidal cumulates: Insights from spinel chemistry. *Am. Min.* 84:1020-1026.

Buchanan P.C., Lindstrom D.J., Mittlefehldt D.W., Koeberl C., Reimold W.U. 2000. The South African polymict eucrite Macibini. *Meteorit. Planet. Sci.* 35:1321-1331.

Burns R.G. 1993. *Mineralogical Applications of Crystal Field Theory, 2nd edition*. New York: Cambridge University Press. 551 p.

Clayton R.N. and Mayeda T.K. 1996. Oxygen isotope studies of achondrites. *Geochim. Cosmochim. Acta* 60:1999-2017.

Cloutis E.A. and Gaffey M.J. 1991. Pyroxene spectroscopy revisited: Spectral-compositional correlations and relationship to geothermometry. *J. Geophys. Res.* 96:22,809-22,826.

Cloutis E.A., Gaffey M.J., Smith D.G.W., and Lambert R.St.J. 1990a. Metal silicate mixtures: Spectral properties and applications to asteroid taxonomy. *J. Geophys. Res.* 95:8323-8338.

Cloutis E.A., Gaffey M.J., Smith D.G.W., and Lambert R.St.J. 1990b. Reflectance spectra of mafic silicate-opaque assemblages with applications to meteorite spectra. *Icarus* 84:315-333.

Chennaoui Aoudjehane H. and Jambon A. 2007. Determination of silica polymorphs in eucrites by cathodoluminescence. *Lunar Planet. Sci. XXXVIII***.** Lunar Planet. Inst., Houston. #1714 (abstr.).

Consolmagno G.Y. and Drake M.J. 1977. Composition and evolution of the eucrite parent body: Evidence from rare earth elements. *Geochim. Cosmochim. Acta* 41:1271-1282.

Delaney J.S., and Prinz M. 1984a. The Polymict Eucrites. *J. Geophys. Res.*. 89:C251-C288.

Delaney J.S., Prinz M., Nehru C.E., Stokes C.P. 1984b. Allan Hills A81001, cumulate eucrites and black clasts from polymict eucrites. *Lunar Planet. Sci.* VX:212-213.

Drake M.J. 2001. The eucrite/Vesta story. *Meteorit. Planet. Sci.* 36:501-513.

Duke M.B. 1965. Metallic iron in basaltic achondrites. *J. Geophys. Res.* 70:1523-1529.

Fisk M.R. and Bence A.E. 1980. Experimental crystallization of chrome spinel in FAMOUS basalt 567-1-1. *Earth Planet. Sci. Lett.* 48:111-123.

Floss C., Jolliff B.L., Benedix G.K., Stadermann F.J., and Reid J. 2007. Hammadah al Hamra 193: The first amphibole-bearing winonaite. *Am. Min.* 92:460-467.

Fowler G.W., Papike J.J., Spilde M.N., and Shearer C.K. 1994. Diogenites as asteroidal cumulates: Insights from orthopyroxene major and minor element chemistry. *Geochim. Cosmochim. Acta* 18:3921-3929.

Gaffey M.J. 1976. Spectral reflectance characteristics of the meteorite classes. *J. Geophys. Res.* 81:905-920.

Gaffey M.J. 1997. Surface lithologic heterogeneity of asteroid 4 Vesta. *Icarus* 127:30-157.

Gooding J.L., Prinz M., and Keil K. 1979. Mineralogy and petrology of the Chervony Kut eucrite. *Proc. Lunar Planet. Sci. X*:446-448.

Greenwood R.C., Frachi I,A., Jambon A., Buchanan P.C. 2005. Widespread magma oceans on asteroidal bodies in the early Solar System. *Nature* 435:916-918.

Grossman J.N. 1994. The Meteoritical Bulletin, no. 76, 1994 January: The U.S. Antarctic meteorite collection. *Meteorit.* 29:100-143.

Hill R. and Roeder P. 1974. The crystallization of spinel from basaltic liquid as a function of oxygen fugacity. *J. Geol.* 82:709-729.

Hsu W. and Crozaz G. 1996. Mineral chemistry and the petrogenesis of eucrites: I. Noncumulate eucrites. *Geochim. Cosmochim. Acta* 60:4571-4591.

Jarosewich E. 1990. Chemical analyses of meteorites: A compilation of stony and iron meteorite analyses. *Meteorit.* 25:323-337.

John C.M. (2004) Plotting and analyzing data trends in ternary diagrams made easy, *EOS* 85:158. (Also available at http://www.agu.org/eos_elec/000562e.shtml).

Johnson, T.V., and Fanale, F.P. 1973. Optical properties of carbonaceous chondrites and their relationship to asteroids. *J. Geophys. Res.* 78:8507-8518.

Kaneda K. and Warren P.H. 1998. Iron-nickel metal-bearing unique eucrite elephant moraine 92023: Its petrography, siderophile concentrations and petrogenesis. *Meteorit. Planet. Sci.*. 33:A81-A82.

Keil K. 2002. Geological history of asteroid 4 Vesta: The “smallest terrestrial planet”. In: *Asteroids III* (eds. W. Bottke, A. Cellino, P. Paolicchi, and R.P. Binzel). Arizona LPI Publishing, pp. 573-585

Kitts K. and Lodders K. 1998. Survey and evaluation of eucrite bulk compositions. *Meteorit. Planet. Sci.* 33:A197-A213.

Lentz R.C.F., Scott E.R.D., and McCoy T.J. 2007. Anomalous eucrites: Using Fe/Mn to search for different parent bodies. *Lunar Planet. Sci. XXXVIII***.** Lunar Planet.. Inst., Houston. #1968 (abstr.).

Mayne R.G., Sunshine J.M., McCoy T.J., and McSween H.Y. 2006. The VISNIR Spectra of Unbrecciated Antarctic Eucrites: A Preliminary Study. *Lunar Planet. Sci. XXXVII*. Lunar Planet. Inst., Houston #1796 (abstr.).

Mason B. (1962) *Meteorites*. J. Wiley and Sons, New York.

McCord T.B., Adams J.B., and Johnson T.V. 1970. Asteroid Vesta: Spectral reflectivity and compositional implications. *Science* 168:1445-1447

McCoy T.J., Ketcham R.A., Wilson L., Benedix G.K., Wadhwa M., and Davis A.M. 2006. Formation of vesicles in asteroidal basaltic meteorites. *Earth Planet. Sci. Lett.* 246:102-108.

Misawa K., Yamaguchi A., and Kaiden H. 2005. U-Pb and ^{207}Pb-^{206}Pb ages of zircons from basaltic eucrites: Implications for early basaltic volcanism on th eucrite parent body. *Geochim. Cosmochim. Acta* 69:5847-5861.

Mittlefehldt D.W. 1994. The genesis of diogenites and HED parent body petrogenesis. *Geochim. Cosmochim. Acta* 58:1537-1552.

Mittlefehldt D.W. 2005. Ibitira: A basaltic achondrite from a distinct parent asteroid and implications for the Dawn mission. *Meteorit. Planet. Sci.* 40:665-677.

Mittlefehldt D.W. and Galindo C. 2002. Petrology and geochemistry of unbrecciated metamorphosed eucrites. *Meteorit. Planet. Sci.*. 37:A101 (abstr.).

Mittlefehldt D.W. and Lee M.T. 2001. Petrology and geochemistry of unusual eucrite GRA 98098. *Meteorit. Planet. Sci.*. 36:A136 (abstr.).

Mittlefehldt D.W. and Lindstrom M.M. 1991. Generation of abnormal trace element abundances in Antarctic eucrites by weathering processes. *Geochim. Cosmochim. Acta* 55:77-87.

Mittlefehldt D.W. and Lindstrom M.M. 2003. Geochemistry of basaltic eucrites, and Hf and Ta as petrogenetic indicators for altered Antarctic eucrites. *Geochim. Cosmochim. Acta* 67:1911-1935.

Mittlefehldt D.W., McCoy T.J., Goodrich C.A., and Kracher A. 1998. Non-chondritic meteorites from asteroidal bodies. In *Planetary Materials* (ed. J.J. Papike). Washington D.C.: Mineralogical Society of America, pp. 4-1 to 4-195.

Miyamoto M., Mito A., and Takano Y. 1982. An attempt to reduce the effects of black materials from the spectral reflectance of meteorites and asteroids. *Memoirs National. Institute of Polar Research Special Issue* 20:345-361

Newsom H.E., and Drake M.J. 1982. The metal content of the eucrite parent body: Constraints from the partitioning behavior of tungsten. *Geochim. Cosmochim. Acta* 46:2483-2489.

O'Neill C.O. and Delaney J.S. 1982. Zoning of eucritic feldspars. *Meteorit.* 17:265.

Papike J.J., Karner J.M., and Shearer C.K. 2003. Determination of planetary basalt parentage: A simple technique using the electron microprobe. *Am. Min.* 88:469-472.

Papike J.J. 1998. Comparative planetary mineralogy: Chemistry of melt-derived pyroxene, feldspar, and olivine. In: *Planetary Materials* (ed. J.J. Papike). Washington D.C.: Mineralogical Society of America, pp. 7-1 to 7-11.

Pun A. and Papike J.J. 1996. Unequilibrated eucrites and the equilibrated Juvinas eucrite: Pyroxene systematics and major, minor, and trace element zoning. *Am. Min.* 81:1438-1451.

Reid A.M. and Barnard B.M. 1979. Unequilibrated and equilibrated eucrites. *Proc. Lunar Planet. Sci. X:*1019-1021.

Righter, K. and Drake, M.J. 1997. A magma ocean on Vesta: Core formation and petrogenesis of eucrites and diogenites. *Meteorit. Planet. Sci.* 32:929-244.

Roeder P.L. and Reynolds I. 1991. Crystallization of chromite and chromium stability in basaltic melts. *J. Pet.* 32:909-934.

Russell C.T., Coradini A., Feldman W.C., Jaumann R., Konopliv A.S., McCord T.B., McFadden L.A., McSween Jr. H.Y., Mottola S., Neukum G., Pieters C.M., Raymond C.A., Smith D.E., Sykes M.V., Williams B.G., and Zuber M.T. 2002. Dawn: A journey to the beginning of the solar system. *Proc. ACM Conf.* pp. 63-66.

Russell C.T., Capaccioni F., Coradini A., Christensen U., De Sanctis M.C., Feldman W.C., Jaumann R., Keller H.U., Konopliv A., McCord T.B., McFadden L.A., McSween H.Y., Mottola S., Neukum G., Pieters C.M., Prettyman T.H., Raymond C.A., Smith D.E., Sykes M.V., Williams B., and Zuber M.T. 2006. Dawn discovery mission to Vesta and Ceres: Present status. *Adv. Space Res.* 38:2043-2048.

Ruzicka A., Synder G.A., and Taylor L.A. 1997. Vesta as the howardite, eucrite, and diogenite parent body: Implications for the size of a core and for large-scale differentiation. *Meteorit. Planet. Sci.* 32:825-840.

Snetsinger K.G., Bunch T.E., and Keil K. 1968. Electron microprobe analysis of vanadium in the presence of titanium. *Am. Min.* **53**, 1770-1773.

Srinivasan G., Whitehouse M.J., Weber I., and Yamaguchi A. 2007. *Science* 317:345-347.

Steele I.M. and Smith I.M. 1976. Mineralogy of the Ibitira eucrite and comparison with other eucrites and lunar samples. *Earth Planet. Sci. Lett.* 33:67-78.

Stolper E. 1977. Experimental petrology of eucritic meteorites. *Geochim. Cosmochim. Acta* 41:587-611.

Takeda H. and Graham A.L. 1991. Degree of equilibration of eucritic pyroxenes and thermal metamorphism of the earliest planetary crust. *Meteorit.* 26:129-134.

Treiman A.H., Lanzirotti A., and Xirouchakis D. 2004. Ancient water on asteroid 4 Vesta: evidence from a quartz veinlet in the Serra de Magé eucrite meteorite. *Earth Planet. Sci. Lett.* 219:189-199.

Wadhwa M., Srinivasan G., and Carlson R.W. 2006. Timescales of planetary differentiation in the early solar system. In: *Meteorites and the Early Solar System II* (eds. D.S. Lauretta and H.Y. McSween Jr.) University of Arizona Press, pp. 715-733.

Warren P.H., Kallemeyn G.W., and Arai T. 1996. Compositional investigation of quench-textured eucrites: Microporphyritic ALH 81001 and vesicular PCA 91007. *LPI Tech. Rep. 96-02*, 1:35-36.

Wiechert U.H., Halliday A., Palme H., and Rumble D. 2004. Oxygen isotope evidence for rapid mixing of the HED meteorite parent body. *Earth Planet. Sci. Lett.* 221:373-382.

Wilkening L.L. and Anders E. 1975. Some studies of an unusual eucrite – Ibitira. *Geochim. Cosmochim. Acta* 39*:1205-1210.*

Yamaguchi A. 2000. Spinels in basaltic eucrites: Implication for crystallization and metamorphic history. *Meteorit. Planet. Sci.*. 35:A174 (abstr.).

Yamaguchi A. and Mikouchi T. 2005. Heating Experiments of the HaH 262 eucrite and implication for the metamorphic history of highly metamorphosed eucrites. *Lunar Planet. Sci. XXXVI***.** Lunar Planet. Inst., Houston. #1574 (abstr.).

Yamaguchi A., Taylor G.J., and Keil K. 1996. Global crustal metamorphism of the eucrite parent body. *Icarus* 124:97-112.

Yamaguchi A., Taylor G.J., Keil K., Bogard D.D. 1997a. Evidence for a large cratering event on the HED parent body (Vesta) ~4.5 GA ago. *Meteorit. Planet. Sci.* 32:A144-A155.

Yamaguchi A., Taylor G.J., and Keil K. 1997b. Metamorphic history of the eucritic crust of 4 Vesta. *J. Geophys. Res.* 102:13,381-13,386.

Yamaguchi A., Taylor G.J., and Keil K. 1997c. Shock and thermal history of equilibrated eucrites from Antarctica. *Ant. Met. Res.* 10:431-453.

Yamaguchi A., Taylor G.J., Keil K., Floss C., Crozaz G., Nyquist L.E., Bogard D.D., Garrison D.H., Reese Y.D., Weismann H, and Shih C-Y. 2001. Post-crystallization reheating and partial melting of eucrite EET 90020 by impact into

the hot crust of asteroid 4Vesta ~4.50Ga. *Geochim. Cosmochim. Acta* 65:3577-3599.

Electronic Annex Caption

SEM Mineral Maps of the Unbrecciated Eucrites

Figure Captions

1. Compiled SEM mineral maps for six unbrecciated eucrites showing the wide range of textures seen within the samples studied. Each map consists of superimposed Fe, Si, and Al elemental X-ray maps. Blue/purple – pyroxene, lilac – plagioclase, green – silica, red – oxides, sulfides and metal. (a) QUE 94484. (b) ALH A81001. (c) Chervony Kut. (d) Ibitira. (e) GRA 98098. (f) Serra de Magé

2. Back-scattered electron images of unbrecciated eucrites. (a) Radiating laths of skeletal pyroxene in ALH A81001. (b) Pyroxene phenocrysts in ALH A81001. (c) Fine-grained ilmenite found scattered throughout ALH A81001. (d) Chervony Kut showing cataclastic texture. (e) Mesostasis assemblage in QUE 94484. Abbreviations used: Tr = troilite, Ilm = ilmenite, Plag = plagioclase, Px = pyroxene, and SiO_2 = silica.

3. A comparison of the relative modal abundances of plagioclase and pyroxene in the unbrecciated eucrites. Basaltic samples are denoted by crosses and the cumulate eucrites by triangles.

4. Major (quadrilateral) and minor (Al, Cr, Ti) element compositions in pyroxenes of the unbrecciated eucrites.

5. Primary chemical zoning trends of pyroxene, after Pun and Papike (1996). (a) Mg-Fe-Ca trend. Mg-rich cores to Fe-rich rims. (b) Mg-Fe trend. (c) Fe-Ca trend, showing tie lines between host pigeonite to exsolved augite in ordinary eucrites. These are considered to be equilibrated, as chemical zoning is no longer present.

6. All pyroxene elemental composition analyses and ratio plots for the unbrecciated eucrites studied. (a) Fe/Mn versus Fe/Mg. (b) Fe/Mn versus Wo content. All values plotted here are above the detection limit on the electron microprobe. Counting errors lead to a 2σ of $\pm 9.7\%$ for Fe/Mn, due to the larger counting error for Mn, which is only a minor element in eucrite pyroxenes. This error still does not account for the distinct Fe/Mn ratio seen in QUE 94484 in all three of these plots

7. Anorthite (An) ranges for plagioclase analyses in the unbrecciated eucrites. Basaltic eucrites are shown using filled-in black bars and the cumulate eucrites with unfilled bars.

8. Elemental compositions of plagioclase in the unbrecciated eucrites studied. (a) K (atoms per formula unit) vs. An content. Lines defining trends for Moon/Vesta, Mars and Earth are taken from Papike (1998). (b) Fe (atoms per formula unit) vs. An content. The detection limits of these elements on the electron microprobe are 0.003 afu for K and 0.001 afu for Fe. The previous reported Fe content for eucrite pyrxoenes of <0.06 afu is shown (Papike, 1998).

9. All spinel analyses for the unbrecciated eucrites studied. (a) All basaltic eucrites in this study. (b) All cumulate eucrites in this study. (c) All analyses compared to the spinel compositions of the petrographic types of Yamaguchi. The grey arrows indicate the compositional trends with increasing crystallization.

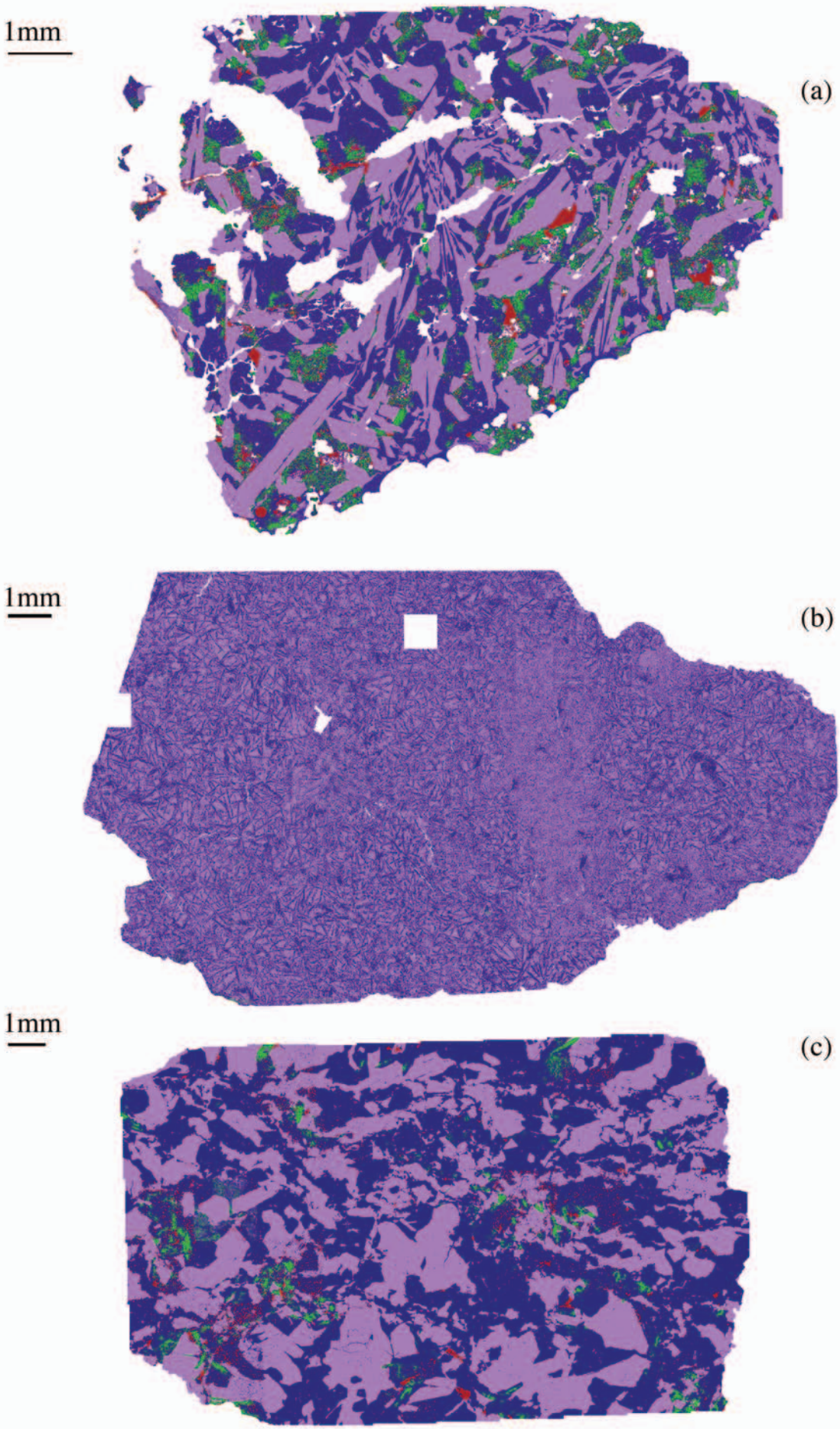

W5195 - Figure 1 - Mayne et al.

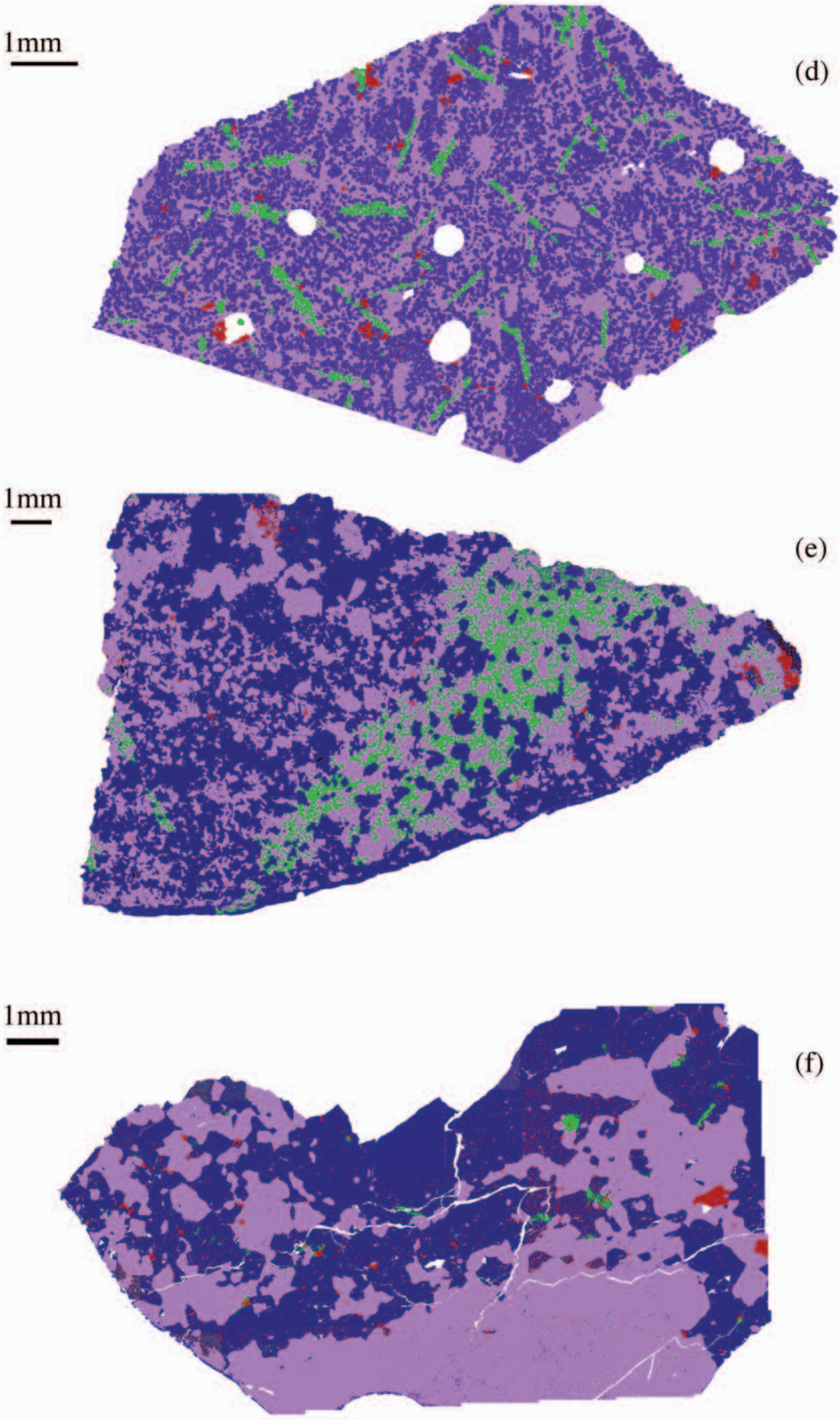

W5195 - Figure 1 continued - Mayne et al.

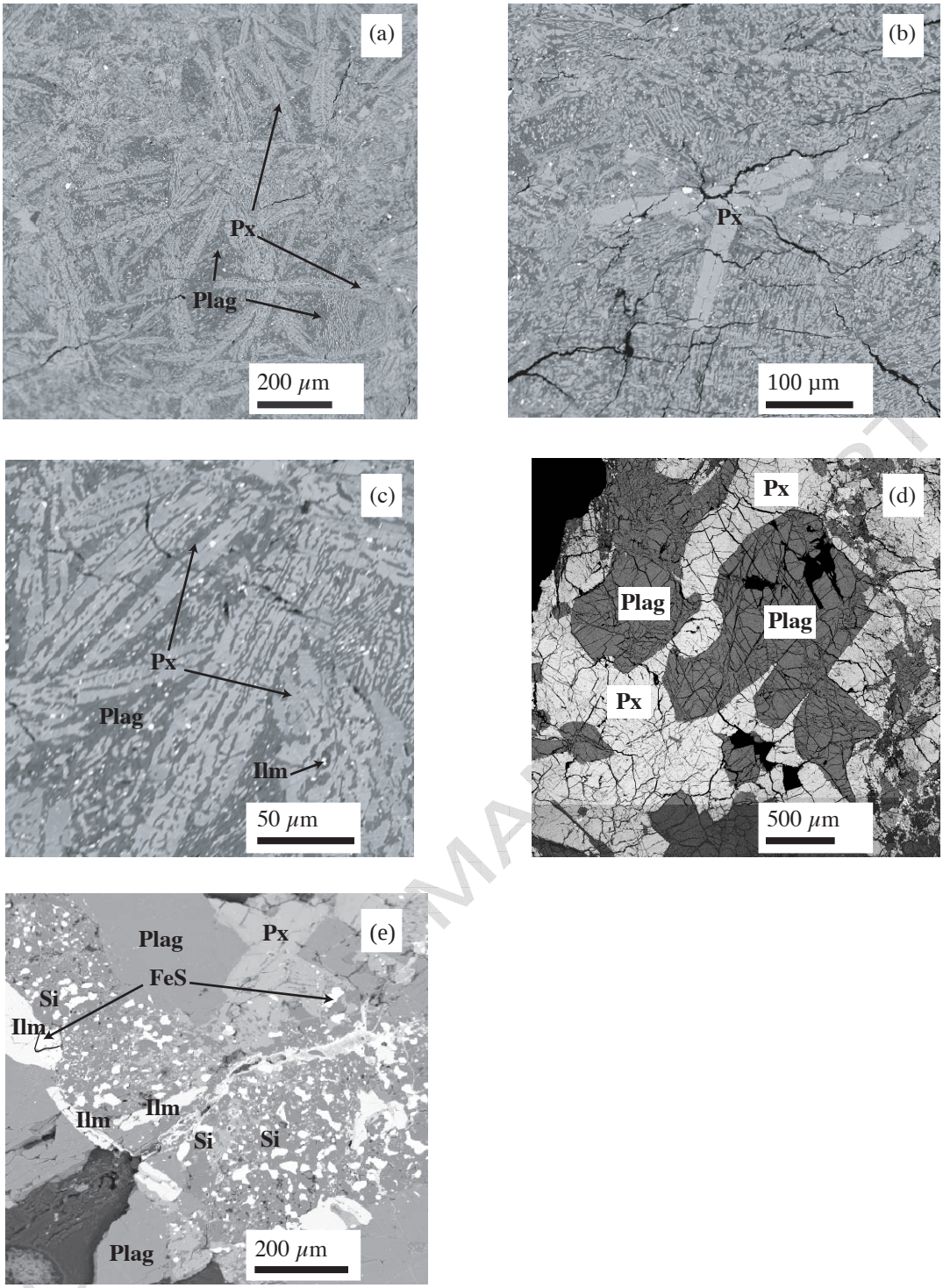

W5195 - Figure 2 - Mayne et al.

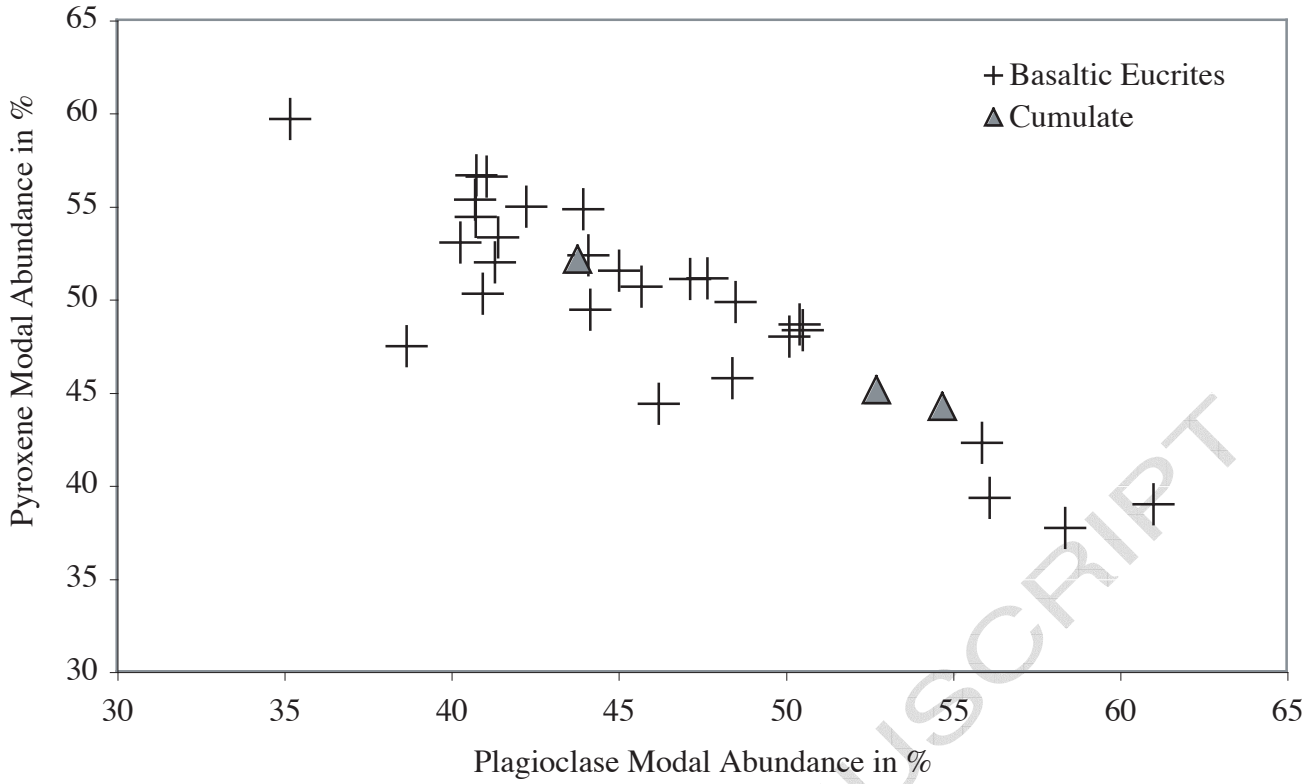

W5195 - Figure 3 - Mayne et al.

Cumulate Eucrites

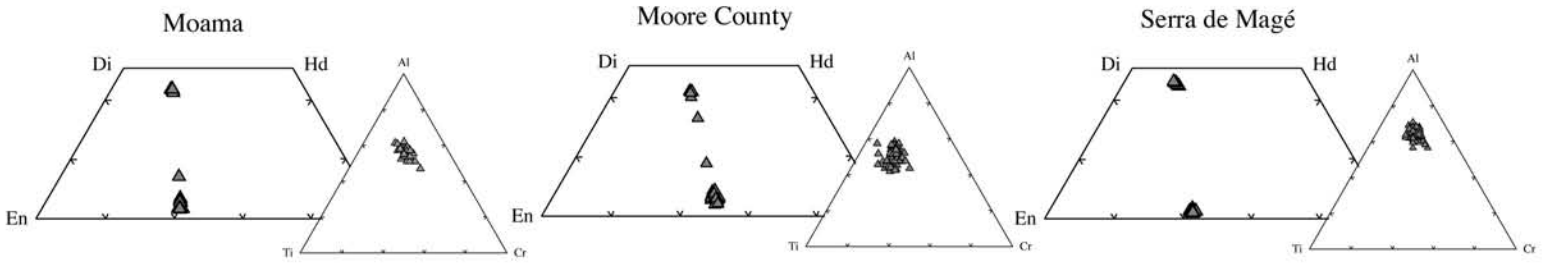

Basaltic Eucrites

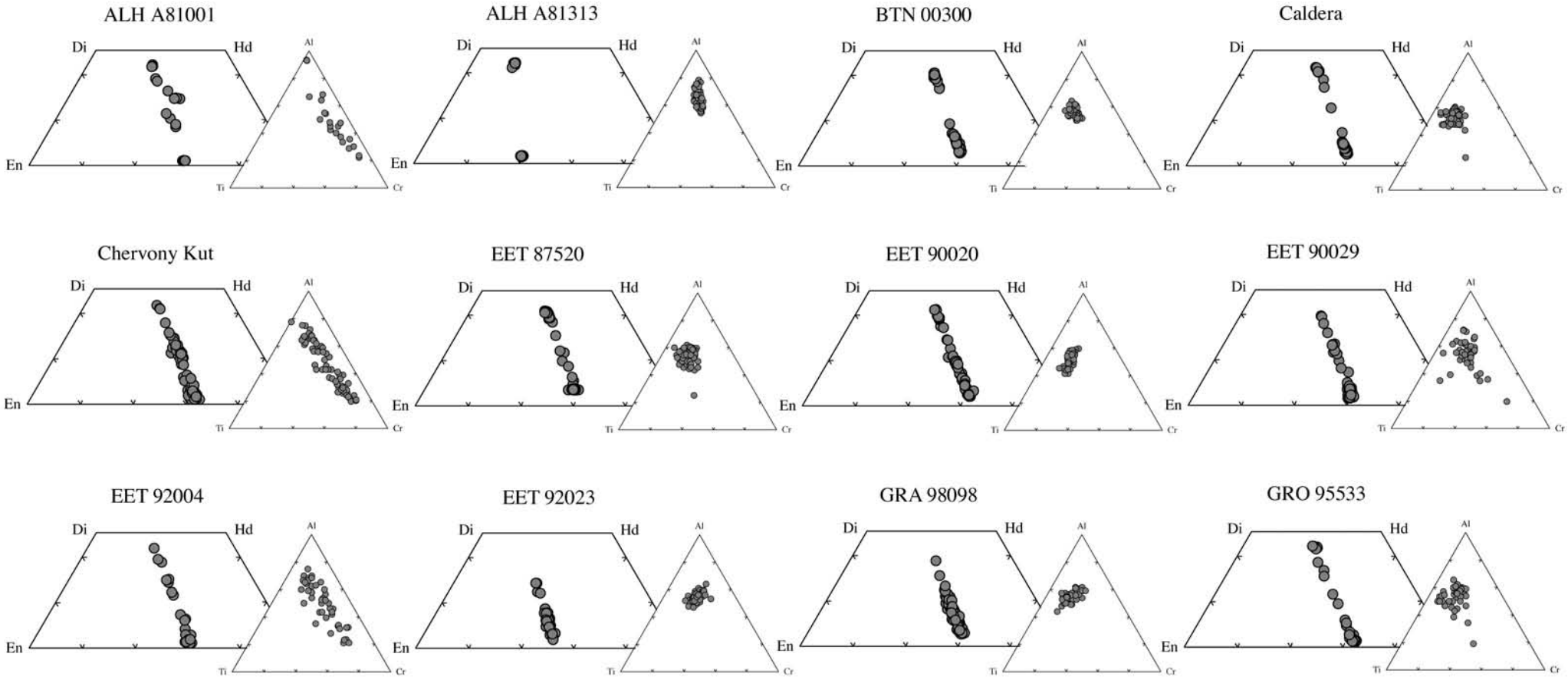

W5195 - Figure 4 - Mayne et al.

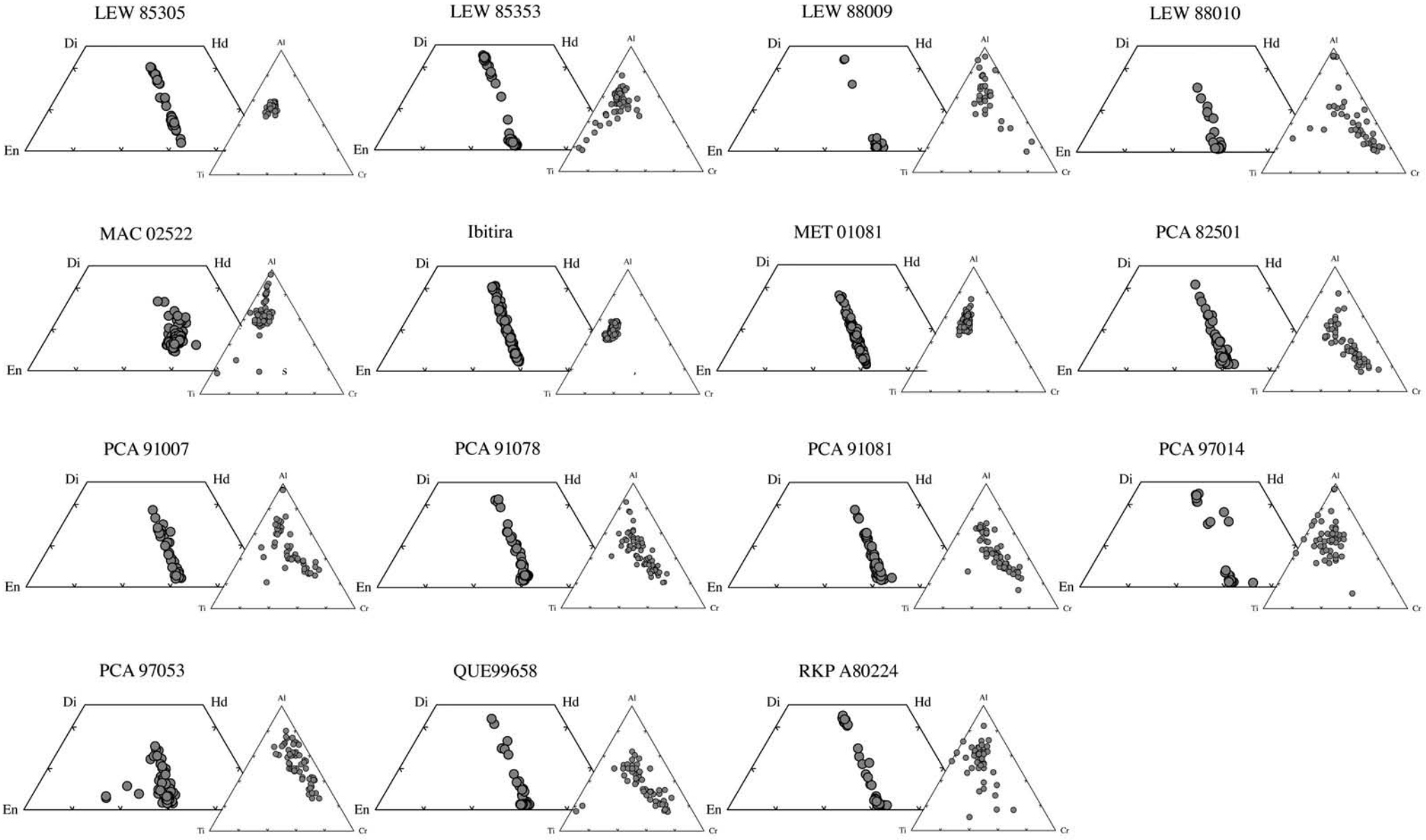

W5195 - Figure 4 continued - Mayne et al.

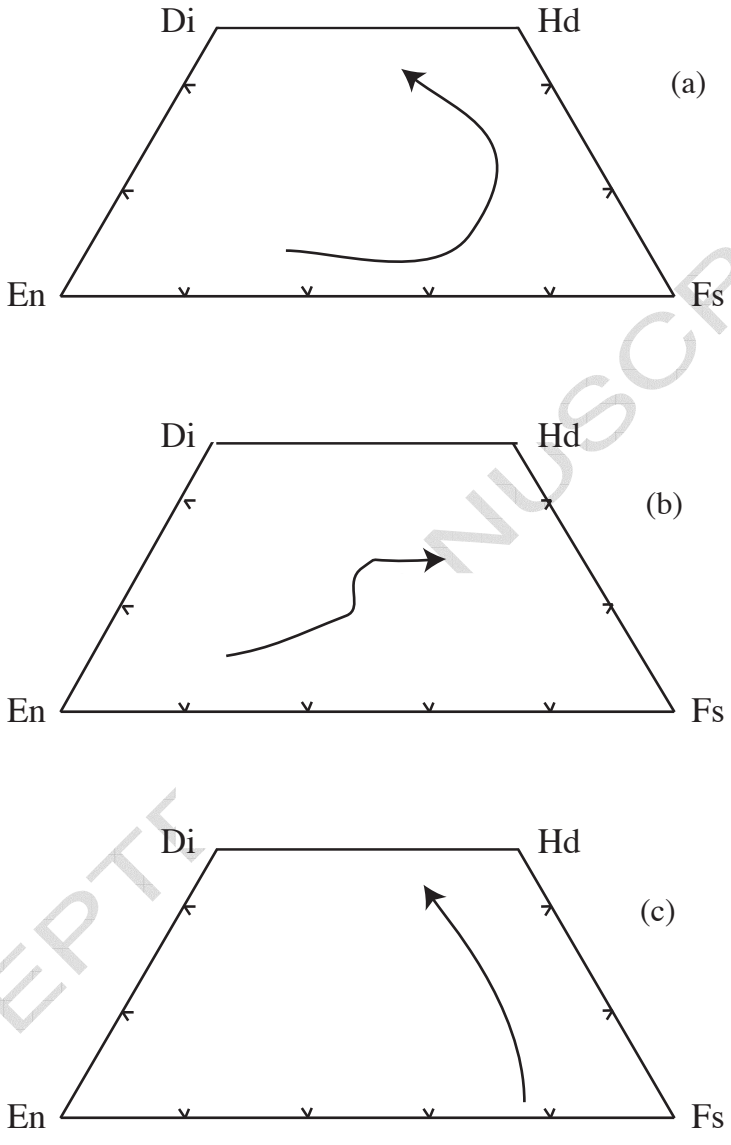

W5195 - Figure 5 - Mayne et al.

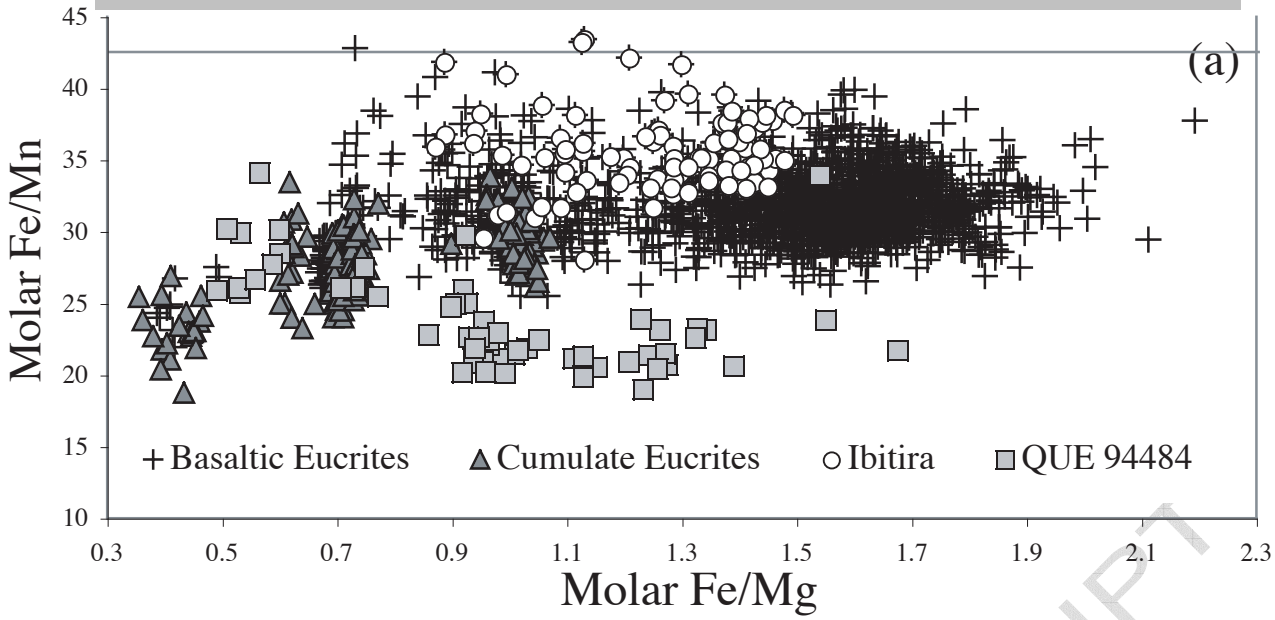

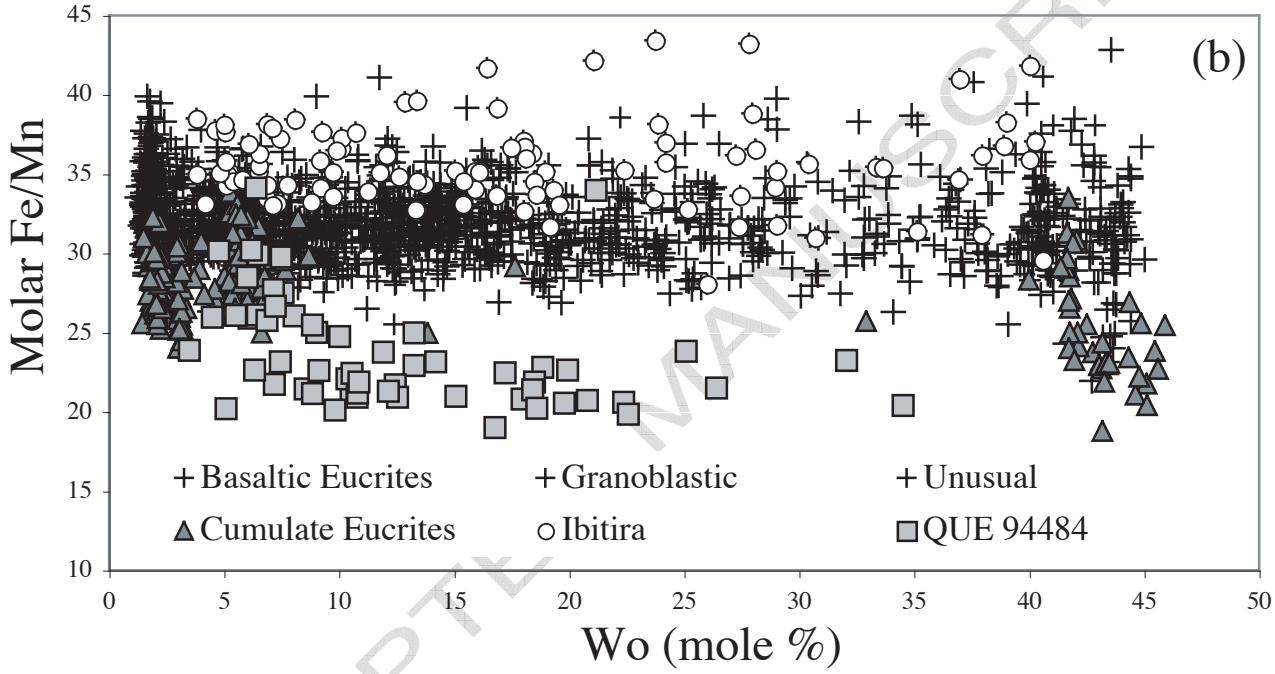

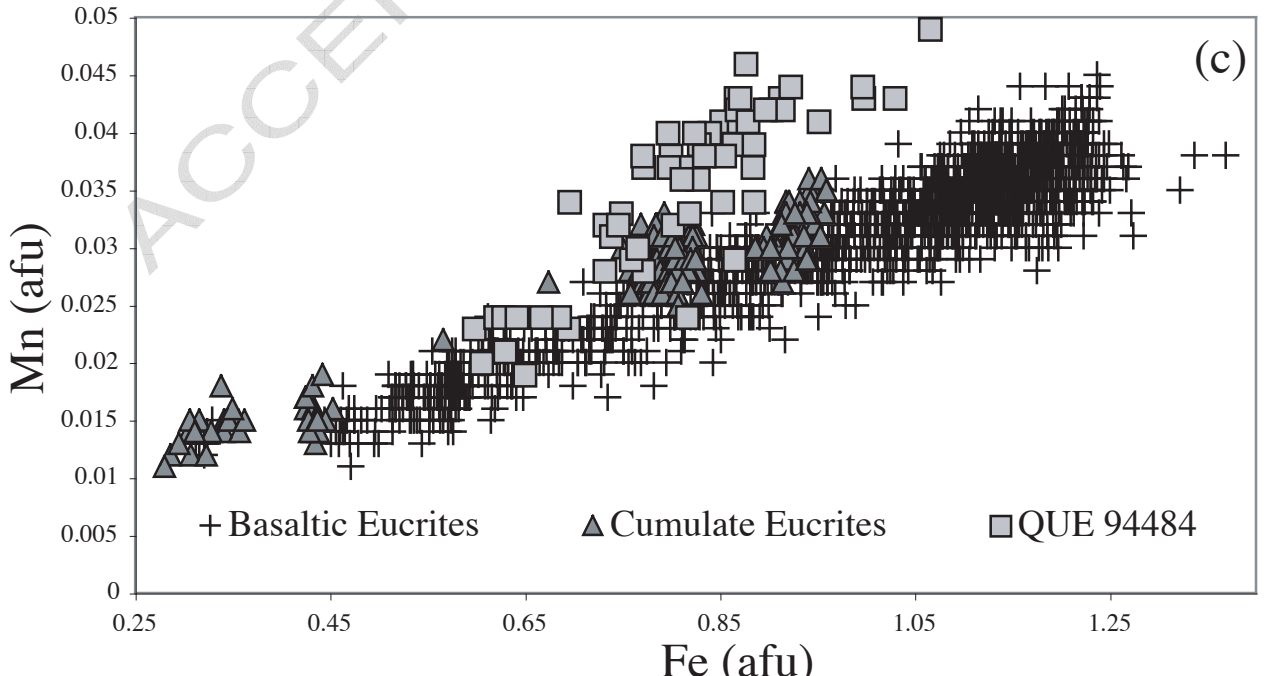

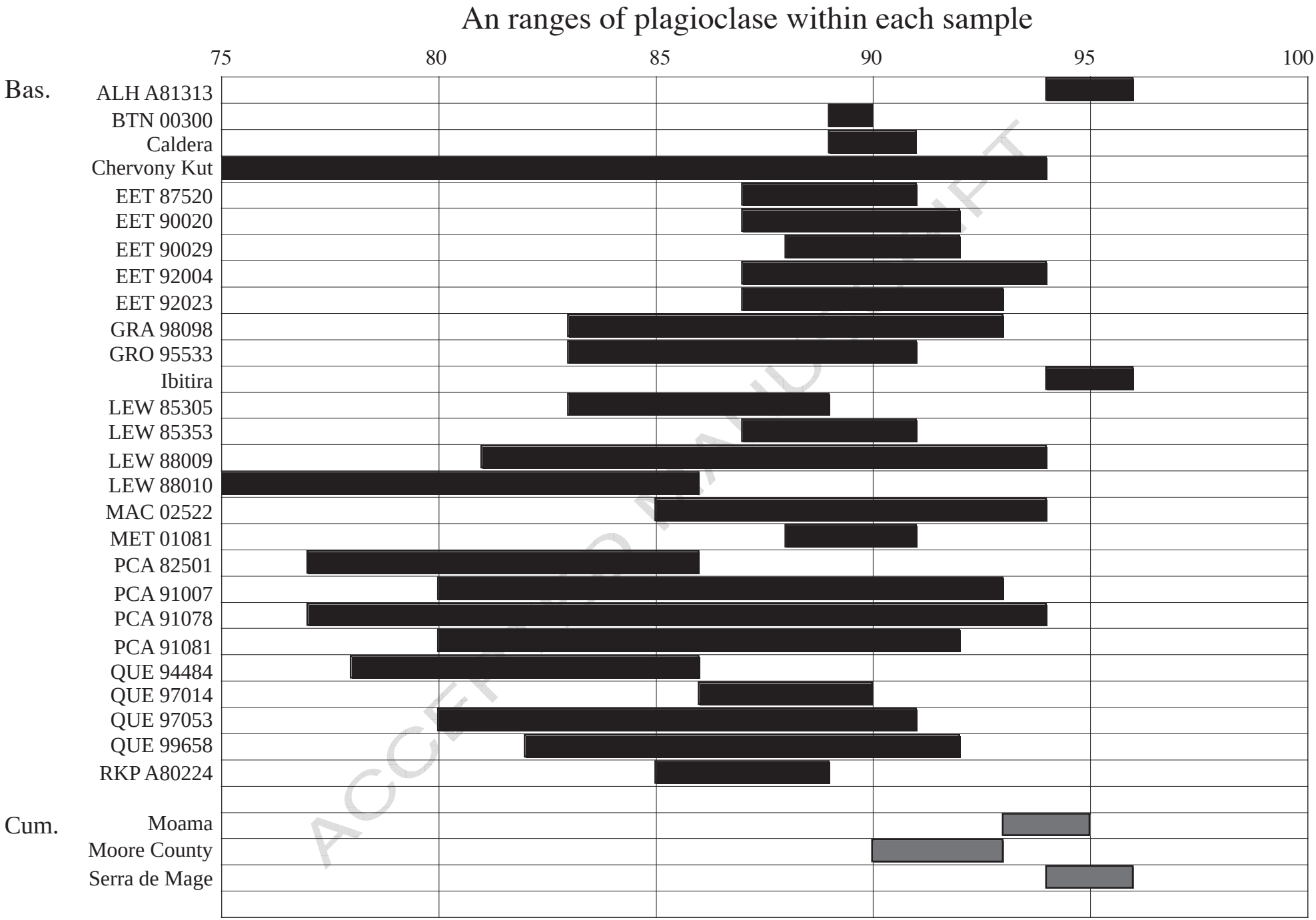

W5195 - Figure 7 - Mayne et al.

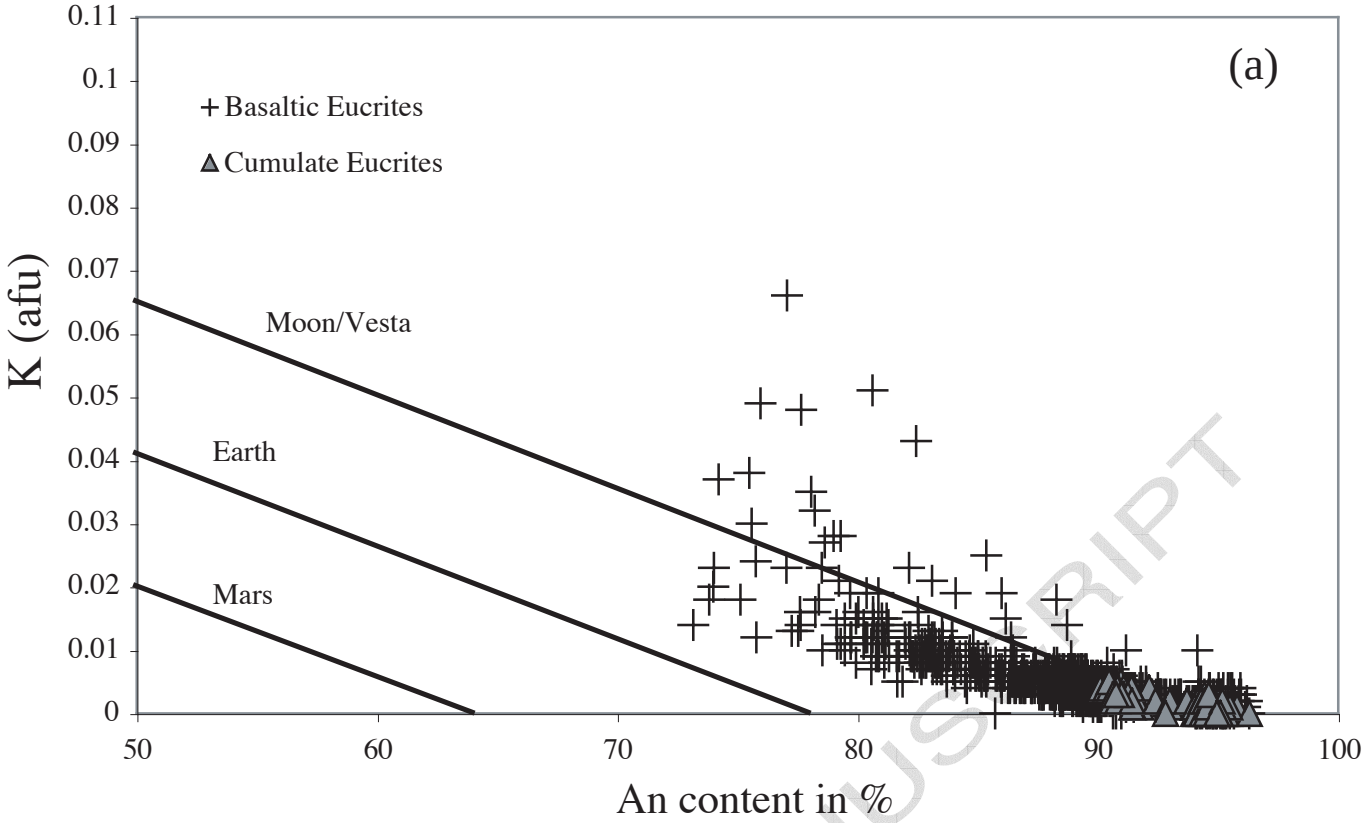

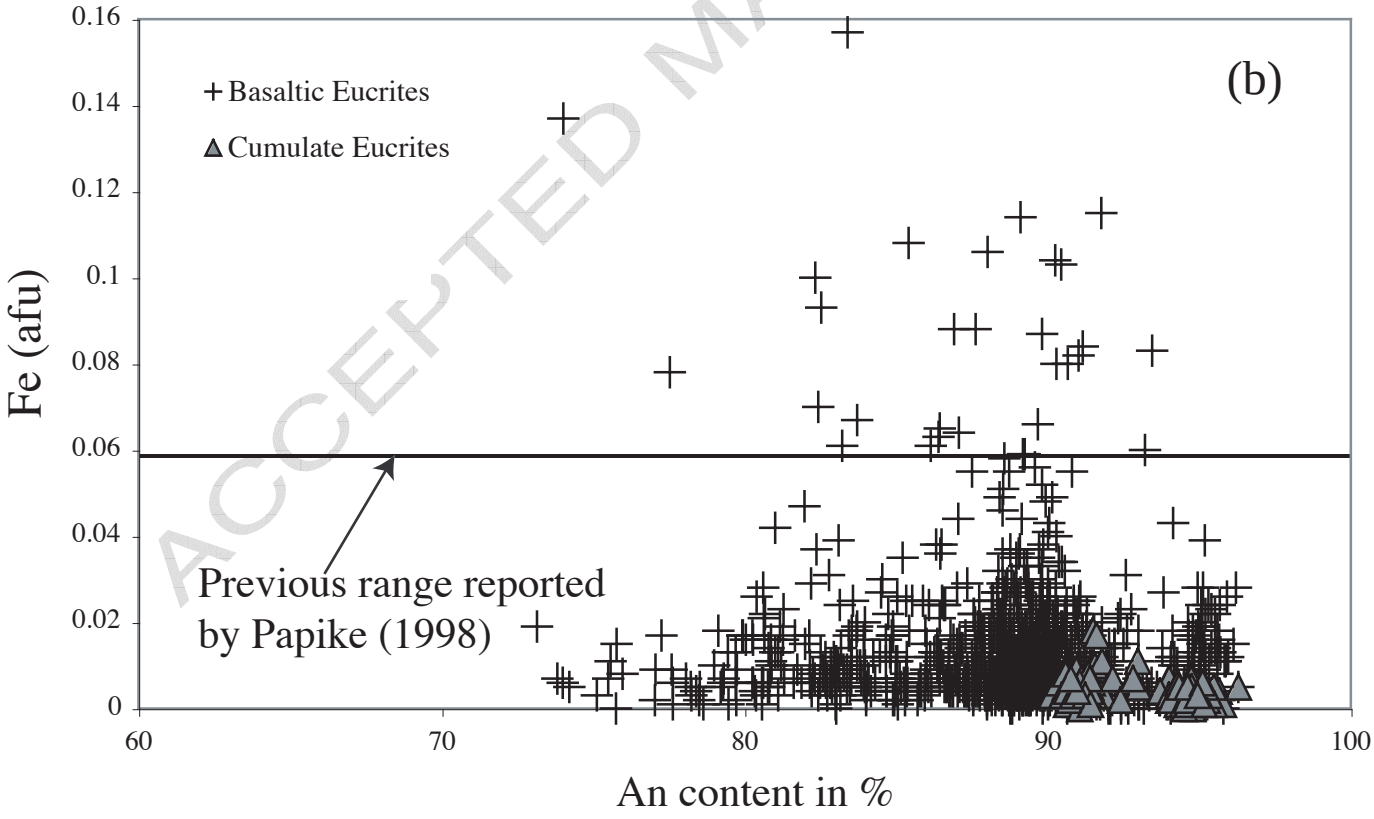

W5195 - Figure 8 - Mayne et al.

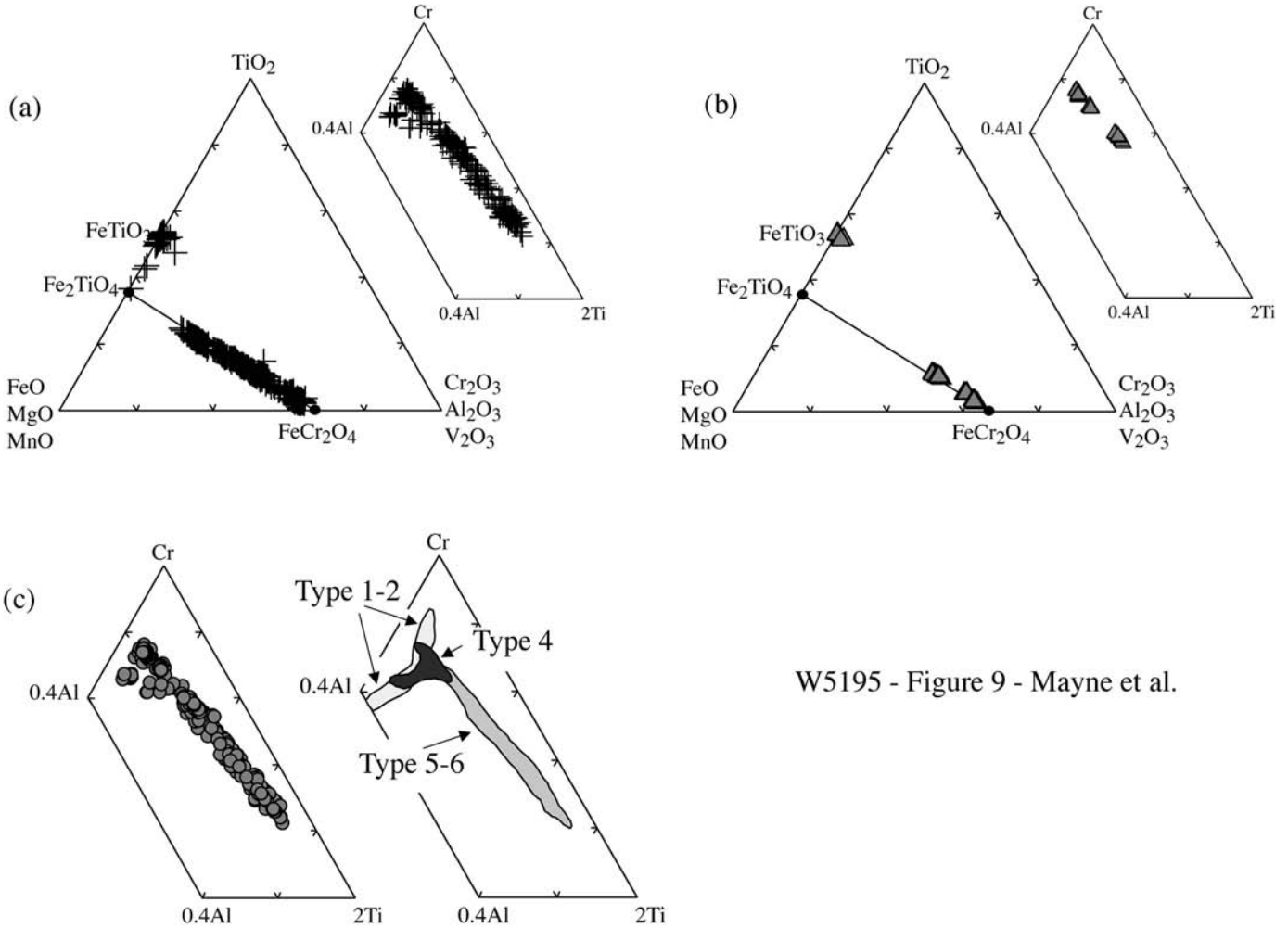

W5195 - Figure 9 - Mayne et al.

Table 1: Eucrite samples examined in this study. Thin-section numbers are given where available.

Sample	Section Number	SEM map Magnification	Sample Description
ALH A81001	10	70	Vitrophyric, skeletal pyroxene, few pyroxene micriphenocrysts
ALH A81313	1	40	Only sample with maskelynite, coarse-grained
BTN 00300	26	37	Granoblastic, some igneous texture remains, a few tabular silica grains
Caldera	USNM 6394-2	45	Gabbroic
Chervony Kut	USNM 6529-1	40	Sub-ophitic, highly fractured (shock)
EET 87520	18	37	Cumulate texture, coarse-grained
EET 90020	7	37	Predominantly equigranular, granoblastic
EET 90029	3	37	Microcrystalline, acicular plagioclase, shock veins
EET 92004	7	37	Sub-ophitic, fractured (shock)
EET 92023		35	Equigranular, cumulate
GRA 98098	18	30	Poikilitc quartz grain, inequigranular, granoblastic
GRO 95533	2	33	Granulated pyroxene, shocked, plagioclase undulose extinction
Ibitira	USNM 6153-1	100	Vesicular, granoblastic, tabular silica grains
LEW 85305		33	Possible poikilitc quartz grain
LEW 85353		40	Shock veins, granulated pyroxene
LEW 88009		80	Ophitic, acicular plagioclase
LEW 88010		40	Ophitic, variolitic plagioclase
MAC 02522	11	37	Pyroxene mosaicized, ophiticto sub-ophitic texture
MET 01081	14	37	Shock mosaicism of pyroxene and plagioclase
Moama	USNM 6376-1	4	Fine-grained cumulate
Moore County	USNM 929-5	40	Cumulate, some plagioclase poikilitically enclosed by pyroxene
PCA 82501		45	Sub-ophitic, fractured (shock)
PCA 91078	8	37	Sub-ophitic, coarse-grained
QUE 94484		50	Sub-ophitic, late-stage phases/mesostasis abundant, spherulitic plagioclase
QUE 97014		45	Ophitic, fractured (shock)
QUE 97053	6	43	Sub-ophitic, shocked, moasicized pyroxene, undulose plagioclase
QUE 99658	2	45	Sub ophitic, spherulitic plagioclase, shock veins. Fractured
RKP A80224	2	45	Ophitic, pyroxene partially mosaicized
Serra de Magé	USNM 839-3	45	Coarse grained cumulate

Table 2: Average modal abundances of the twenty-nine unbrecciated eucrites studied[a]

	ALH A81001	ALH A81313	BTN 00300	CALDERA	CHERVONY KUT	EET 87520	EET 90020	EET 90029
Plagioclase	61 (2)	48 (0)	48 (0)	39 (0)	45 (0)	49 (0)	50 (0)	56 (0)
Pyroxene	39 (2)	51 (0)	46 (0)	47 (0)	52 (0)	50 (0)	49 (0)	39 (0)
Silica	0 -	<1 (0)	5 (0)	12 (0)	2 (0)	1 (0)	<1 (0)	4 (0)
OSM	0 -	<1 (0)	1 (0)	1 (0)	1 (0)	0 (0)	<1 (0)	<1 (0)

	EET 92004	EET 92023	GRA 98098	GRO 95533	IBITIRA	LEW 85305	LEW 85353	LEW 88009
Plagioclase	44 (0)	42 (0)	41 (0)	44 (0)	41 (0)	35 (0)	41 (0)	47 (0)
Pyroxene	55 (0)	55 (0)	50 (0)	52 (0)	53 (0)	60 (0)	54 (0)	51 (0)
Silica	<1 (0)	2 (0)	8 (0)	2 (0)	4 (0)	3 (2)	4 (0)	2 (0)
OSM	<1 (0)	1 (0)	<1 (0)	1 (0)	<1 (0)	2 (2)	1 (0)	0 (0)

	LEW88010	MAC 02522	MET 01081	MOAMA	MOORE COUNTY	PCA 82501	PCA 91007	PCA 91078
Plagioclase	41 (0)	41 (0)	40 (0)	55 (0)	44 (0)	44 (0)	41 (2)	46 (0)
Pyroxene	55 (0)	57 (0)	53 (0)	44 (0)	52 (0)	49 (0)	57 (2)	51 (0)
Silica	3 (0)	2 (0)	5 (0)	<1 (0)	3 (0)	5 (0)	2 (0)	3 (0)
OSM	1 (0)	<1 (0)	1 (0)	<1 (0)	<1 (0)	2 (0)	<1 (0)	<1 (0)

	PCA 91081	QUE 94484	QUE 97014	QUE 97053	QUE 99658	RKP A80224	SERRA DE MAGE
Plagioclase	56 (1)	46 (1)	58 (0)	51 (0)	50 (0)	41 (0)	53 (0)
Pyroxene	42 (1)	44 (1)	38 (0)	48 (0)	48 (0)	52 (0)	45 (0)
Silica	2 (0)	7 (0)	3 (0)	<1 (0)	1 (0)	4 (1)	<1 (0)
OSM	0 (0)	2 (0)	<1 (0)	<1 (0)	<1 (0)	3 (1)	1 (0)

[a]Figures in parentheses represent 1σ errors in the average modal abundance measurement, calculated from the variations between the three individual mode measurements.

Table 3: Representative pyroxene analyses[a].

	ALH A81001		ALH A81313		BTN 00300		Caldera		Chervony Kut		EET 87520		EET 90020	
	Low-Ca	High-Ca	Low-Ca	High-Ca	Low-Ca	High-Ca	Low-Ca	High-Ca	Low-Ca	High-Ca	Low-Ca	High-Ca	Low-Ca	High-Ca
SiO2	49.8	50.3	52.9	52.4	49.3	50.3	49.9	50.7	48.3	50.2	49.5	50.3	49.2	50.0
TiO2	0.09	0.33	0.21	0.30	0.25	0.44	0.36	0.74	0.37	0.32	0.21	0.47	0.51	1.03
Al2O3	0.27	0.70	0.43	0.94	0.31	0.66	0.27	0.84	0.46	0.94	0.21	0.79	0.49	1.29
Cr2O3	0.26	0.94	0.23	0.33	0.19	0.29	0.08	0.33	1.55	0.39	0.12	0.39	0.19	0.47
MgO	13.4	10.7	20.0	14.1	11.6	9.8	12.1	9.9	11.7	10.1	11.9	10.1	11.2	9.63
CaO	0.63	20.7	1.31	20.7	2.96	17.8	3.12	19.6	1.86	13.2	3.03	18.8	2.21	17.6
MnO	1.07	0.44	0.83	0.48	0.99	0.65	1.12	0.55	1.11	0.74	1.11	0.56	1.13	0.63
FeO	34.1	15.0	24.1	10.5	33.9	19.4	33.3	17.4	34.7	24.5	33.6	17.8	35.3	19.4
Na2O	<0.03	0.05	<0.03	0.07	0.03	0.06	<0.03	0.07	<0.03	<0.03	0.03	0.08	<0.03	0.10
Total	99.57	99.06	99.94	99.72	99.60	99.35	100.24	100.12	100.04	100.39	99.68	99.19	100.27	100.11
Si	1.98	1.95	1.99	1.97	1.98	1.97	1.98	1.96	1.94	1.97	1.98	1.96	1.97	1.94
Ti	0.00	0.01	0.01	0.01	0.01	0.01	0.01	0.02	0.01	0.01	0.01	0.01	0.02	0.03
Al	0.01	0.03	0.02	0.04	0.02	0.03	0.01	0.04	0.02	0.04	0.01	0.04	0.02	0.06
Cr	0.01	0.03	0.01	0.01	0.01	0.01	0.00	0.01	0.05	0.01	0.00	0.01	0.01	0.01
Mg	0.80	0.62	1.12	0.79	0.69	0.57	0.72	0.57	0.70	0.59	0.71	0.59	0.67	0.56
Ca	0.03	0.86	0.05	0.83	0.13	0.75	0.13	0.81	0.08	0.55	0.13	0.79	0.10	0.73
Mn	0.04	0.02	0.03	0.02	0.03	0.02	0.04	0.02	0.04	0.03	0.04	0.02	0.04	0.02
Fe	1.14	0.49	0.76	0.33	1.14	0.64	1.11	0.56	1.17	0.80	1.12	0.58	1.18	0.63
Na	0.00	0.00	0.00	0.01	0.00	0.00	0.00	0.01	0.00	0.00	0.00	0.01	0.00	0.01
Total	4.01	4.01	3.99	4.00	4.01	4.00	4.00	4.00	4.01	4.00	4.01	4.00	4.00	4.00
Wo	1.38	43.7	2.74	42.7	6.48	38.1	6.81	41.7	4.11	28.4	6.61	40.2	4.88	38.2
En	40.6	31.4	58.0	40.4	35.4	29.3	36.6	29.4	35.9	30.3	36.2	30.0	34.4	29.1
Fs	58.0	24.8	39.3	16.9	58.1	32.5	56.6	28.8	60.0	41.3	57.1	29.8	60.7	32.8

	EET 90029		EET 92004		EET 92023		GRA 98098		GRO 95533		Ibitira		LEW 85305	
	Low-Ca	High-Ca	Low-Ca	High-Ca	Low-Ca	High-Ca	Low-Ca	High-Ca	Low-Ca	High-Ca	Low-Ca	High-Ca	Low-Ca	High-Ca
SiO2	49.7	51.4	49.9	51.6	49.9	50.0	49.5	49.8	49.6	50.8	49.8	49.9	49.5	50.6
TiO2	0.22	0.40	0.13	0.23	0.47	0.81	0.49	0.79	0.12	0.27	0.60	1.16	0.44	0.52
Al2O3	0.24	0.47	0.17	0.46	0.56	1.23	0.54	1.12	0.13	0.48	0.40	1.44	0.48	0.73
Cr2O3	0.12	0.15	0.38	0.40	0.23	0.69	0.25	0.44	0.02	0.24	0.18	0.42	0.22	0.34
MgO	12.4	10.3	12.4	11.0	14.8	13.8	11.8	10.9	11.5	9.50	12.8	10.2	10.6	9.46
CaO	1.18	18.0	0.97	18.2	2.73	11.0	2.93	10.8	0.85	20.3	2.33	19.0	5.98	18.7
MnO	1.10	0.61	1.16	0.52	0.87	0.65	1.12	0.77	1.13	0.62	0.95	0.57	1.05	0.62
FeO	34.7	18.4	35.1	17.9	29.6	21.1	33.3	25.3	36.2	17.0	33.2	17.4	32.0	19.4
Na2O	<0.03	0.07	<0.03	0.06	<0.03	0.09	0.04	0.09	<0.03	0.05	<0.03	0.05	0.05	0.11
Total	99.72	99.88	100.12	100.30	99.20	99.46	99.97	99.87	99.56	99.24	100.24	100.03	100.35	100.54
Si	1.99	1.99	1.99	1.98	1.97	1.94	1.97	1.95	2.00	1.98	1.97	1.93	1.97	1.96
Ti	0.01	0.01	0.00	0.01	0.01	0.02	0.02	0.02	0.00	0.01	0.02	0.03	0.01	0.02
Al	0.01	0.02	0.01	0.02	0.03	0.06	0.03	0.05	0.01	0.02	0.02	0.07	0.02	0.03
Cr	0.00	0.01	0.01	0.01	0.01	0.02	0.01	0.01	0.00	0.01	0.01	0.01	0.01	0.01
Mg	0.74	0.59	0.74	0.63	0.87	0.80	0.70	0.64	0.69	0.55	0.76	0.59	0.63	0.55
Ca	0.05	0.75	0.04	0.75	0.12	0.46	0.13	0.45	0.04	0.85	0.10	0.79	0.26	0.78
Mn	0.04	0.02	0.04	0.02	0.03	0.02	0.04	0.03	0.04	0.02	0.03	0.02	0.04	0.02
Fe	1.16	0.60	1.17	0.57	0.98	0.68	1.11	0.83	1.22	0.56	1.10	0.56	1.07	0.63
Na	0.00	0.01	0.00	0.01	0.00	0.01	0.00	0.01	0.00	0.00	0.00	0.00	0.00	0.01
Total	4.00	3.99	4.00	4.00	4.00	4.00	4.00	3.99	4.00	4.00	4.00	4.00	4.00	4.00
Wo	2.57	38.6	2.11	38.4	5.87	23.6	6.46	23.6	1.90	43.4	5.07	40.6	13.1	39.8
En	37.9	30.6	37.8	32.2	44.3	41.1	36.1	33.2	35.5	28.2	38.7	30.4	32.2	28.0
Fs	59.6	30.8	60.1	29.4	49.8	35.3	57.4	43.2	62.6	28.4	56.2	29.0	54.7	32.2

	LEW 85353		LEW 88009		LEW 88010		MAC 02522	MET 01081		Moama		Moore County		PCA 82501	
	Low-Ca	High-Ca	Low-Ca	High-Ca	Low-Ca	High-Ca		Low-Ca	High-Ca	Low-Ca	High-Ca	Low-Ca	High-Ca	Low-Ca	High-Ca
SiO2	49.8	50.5	49.5	52.0	49.5	50.6	48.1	48.7	49.2	52.3	51.9	51.2	51.5	49.0	50.8
TiO2	0.32	0.86	0.17	0.19	0.09	0.59	0.66	0.48	0.70	0.24	0.41	0.36	0.63	0.23	0.33
Al2O3	0.16	1.16	0.18	0.43	0.41	0.33	1.00	0.51	1.06	0.43	0.70	0.27	0.76	0.23	0.38
Cr2O3	0.05	0.20	0.33	0.24	0.77	0.37	0.25	0.25	0.40	0.25	0.35	0.11	0.33	1.42	0.22
MgO	13.3	11.0	12.4	10.4	12.9	11.6	9.63	11.7	11.0	19.6	13.7	15.7	12.2	12.3	10.9
CaO	0.82	21.0	0.73	21.0	0.75	14.4	6.64	2.31	9.68	1.45	21.2	3.06	20.1	1.77	16.6
MnO	1.01	0.43	1.12	0.53	1.07	0.65	0.97	1.07	0.90	0.89	0.49	0.87	0.58	1.07	0.52
FeO	34.7	14.5	35.9	16.1	34.2	20.9	31.9	34.5	26.1	24.9	11.1	28.3	13.9	34.2	19.9
Na2O	<0.03	0.06	<0.03	0.06	<0.03	0.03	0.04	<0.03	0.06	<0.03	0.06	<0.03	0.09	<0.03	0.05
Total	100.22	99.67	100.33	100.89	99.64	99.42	99.18	99.48	99.06	100.07	99.89	99.98	99.96	100.19	99.72
Si	1.98	1.94	1.98	1.99	1.98	1.97	1.95	1.96	1.95	1.98	1.96	1.99	1.96	1.96	1.98
Ti	0.01	0.03	0.01	0.01	0.00	0.02	0.02	0.01	0.02	0.01	0.01	0.01	0.02	0.01	0.01
Al	0.01	0.05	0.01	0.02	0.02	0.02	0.05	0.02	0.05	0.02	0.03	0.01	0.03	0.01	0.02
Cr	0.00	0.01	0.01	0.01	0.02	0.01	0.01	0.01	0.01	0.01	0.01	0.00	0.01	0.05	0.01
Mg	0.79	0.63	0.74	0.59	0.77	0.67	0.58	0.70	0.65	1.11	0.77	0.91	0.69	0.73	0.63
Ca	0.04	0.87	0.03	0.86	0.03	0.60	0.29	0.10	0.41	0.06	0.86	0.13	0.82	0.08	0.69
Mn	0.03	0.01	0.04	0.02	0.04	0.02	0.03	0.04	0.03	0.03	0.02	0.03	0.02	0.04	0.02
Fe	1.15	0.47	1.20	0.51	1.14	0.68	1.08	1.16	0.87	0.79	0.35	0.92	0.44	1.14	0.65
Na	0.00	0.00	0.00	0.00	0.00	0.00	0.00	0.00	0.01	0.00	0.00	0.00	0.01	0.00	0.00
Total	4.01	4.01	4.01	4.00	4.00	4.00	4.01	4.01	4.00	4.00	4.01	4.00	4.00	4.01	4.01
Wo	1.77	44.1	1.58	43.8	1.65	30.8	14.8	5.09	21.4	3.02	43.3	6.49	42.0	3.90	35.2
En	39.9	32.2	37.4	30.1	39.6	34.4	29.8	35.8	33.7	56.7	39.0	46.5	35.4	37.6	32.0
Fs	58.3	23.7	61.0	26.2	58.7	34.8	55.4	59.1	44.9	40.3	17.7	47.0	22.6	58.5	32.8

	PCA 91078		QUE 94484		QUE 97014		QUE 97053		QUE 99658		RKP A80224		Serra de Mage	
	Low-Ca	High-Ca	High-Mg	Low-Mg/Ca	High-Ca	Low-Ca	High-Ca	Low-Ca	High-Ca	Low-Ca	High-Ca	Low-Ca	High-Ca	Low-Ca	High-Ca
SiO2	49.6	50.8	52.4	49.2	49.1	49.4	50.9	50.0	49.5	49.6	51.1	49.3	51.0	52.4	52.9
TiO2	0.18	0.23	0.20	0.26	0.62	0.08	0.34	0.16	0.45	0.08	0.15	0.16	0.19	0.15	0.27
Al2O3	0.24	0.41	1.82	0.84	1.66	0.09	0.54	0.30	1.36	0.09	0.31	0.13	0.44	0.29	0.70
Cr2O3	0.18	0.16	0.94	0.32	0.76	0.01	0.23	0.13	0.47	0.07	0.14	0.06	0.20	0.12	0.29
MgO	12.16	10.1	21.4	10.7	9.59	11.5	10.3	13.0	10.1	11.7	10.4	12.1	10.2	19.6	14.0
CaO	2.79	19.52	2.63	5.64	14.6	0.82	20.5	1.90	13.9	1.51	19.5	1.04	20.4	1.02	22.1
MnO	0.94	0.5	0.77	1.47	0.97	1.11	0.50	0.98	0.83	1.09	0.57	0.99	0.58	0.95	0.38
FeO	33.9	17.74	20.2	32.0	22.7	36.7	16.2	33.9	23.3	36.2	17.6	36.0	16.5	25.3	9.84
Na2O	n.m.	n.m.	<0.03	<0.03	0.05	<0.03	0.07	0.03	0.07	<0.03	0.04	<0.03	0.06	<0.03	0.06
Total	100.04	99.47	100.39	100.41	100.05	99.75	99.55	100.32	99.92	100.35	99.80	99.81	99.52	99.88	100.51
Si	1.98	1.98	1.94	1.96	1.93	1.99	1.97	1.98	1.94	1.99	1.98	1.98	1.98	1.99	1.97
Ti	n.m.	n.m.	0.01	0.01	0.02	0.00	0.01	0.01	0.01	0.00	0.00	0.01	0.01	0.00	0.01
Al	0.01	0.01	0.08	0.04	0.08	0.00	0.03	0.01	0.06	0.00	0.01	0.01	0.02	0.01	0.03
Cr	0.01	0.02	0.03	0.01	0.02	0.00	0.01	0.00	0.02	0.00	0.00	0.00	0.01	0.00	0.01
Mg	0.01	0.01	1.19	0.64	0.56	0.69	0.60	0.77	0.59	0.70	0.60	0.72	0.59	1.11	0.78
Ca	0.72	0.58	0.11	0.24	0.62	0.04	0.85	0.08	0.58	0.07	0.81	0.05	0.85	0.04	0.88
Mn	0.12	0.81	0.02	0.05	0.03	0.04	0.02	0.03	0.03	0.04	0.02	0.03	0.02	0.03	0.01
Fe	0.03	0.02	0.63	1.07	0.75	1.24	0.53	1.12	0.77	1.21	0.57	1.21	0.54	0.81	0.31
Na	1.13	0.58	0.00	0.00	0.00	0.00	0.01	0.00	0.01	0.00	0.00	0.00	0.00	0.00	0.01
Total	4.01	4.00	4.00	4.01	4.01	4.00	4.01	4.01	4.01	4.01	4.01	4.01	4.01	4.00	4.01
Wo	95.01	96.4	5.5	12.4	5.5	12.41	32.0	1.78	43.1	4.07	30.1	3.29	40.8	2.27	43.0
En	0.8	0.8	61.8	32.7	61.8	32.7	29.2	35.2	30.3	38.9	30.5	35.4	30.4	36.6	29.9
Fs	4.2	2.8	32.7	54.8	32.7	54.8	38.7	63.0	26.6	57.0	39.4	61.3	28.8	61.1	27.1

[a]n.m. = not measured

Table 4: Representative analyses for plagioclase.

	ALH A81001	ALH A81313	BTN 00300	Caldera	Chervony Kut	EET 87520	EET 90020	EET 90029	EET 92004	EET 92023	GRA 98098	GRO 95533	Ibitira	LEW 85305	LEW 85353
SiO2	69.8	44.6	45.3	45.4	46.8	45.3	46.5	45.8	47.9	46.0	47.2	45.1	45.1	46.4	45.4
Al2O3	19.0	34.0	34.2	34.0	33.4	34.4	32.7	34.3	32.8	34.4	33.3	34.5	35.0	33.7	34.3
MgO	0.08	<0.03	0.04	<0.03	0.03	<0.03	0.05	<0.03	<0.03	0.04	0.05	<0.03	<0.03	<0.03	<0.03
CaO	10.5	19.7	18.3	18.4	17.5	18.1	18.0	18.4	16.6	18.1	17.4	18.5	19.1	17.5	17.9
FeO	0.92	0.19	0.18	0.19	0.04	0.15	0.45	0.32	0.16	0.14	0.34	0.01	0.50	0.34	0.11
Na2O	0.23	0.60	1.11	0.99	1.61	1.11	1.29	0.97	2.13	1.19	1.64	1.00	0.54	1.49	1.30
K2O	0.03	<0.03	0.05	0.06	0.11	0.10	0.06	0.06	0.19	0.06	0.15	0.07	0.03	0.07	0.05
Total	100.54	99.20	99.23	99.16	99.44	99.17	99.06	99.87	99.70	99.89	100.09	99.18	100.26	99.46	99.07
Si	3.01	2.08	2.10	2.11	2.16	2.11	2.16	2.11	2.20	2.12	2.17	2.10	2.08	2.15	2.11
Al	0.96	1.87	1.88	1.87	1.82	1.88	1.80	1.87	1.78	1.87	1.81	1.89	1.91	1.84	1.88
Mg	0.01	0.00	0.00	0.00	0.00	0.00	0.00	0.00	0.00	0.00	0.00	0.00	0.00	0.00	0.00
Ca	0.48	0.99	0.91	0.92	0.87	0.90	0.90	0.91	0.82	0.89	0.86	0.92	0.94	0.87	0.89
Fe	0.03	0.01	0.01	0.01	0.00	0.01	0.02	0.01	0.01	0.01	0.01	0.00	0.02	0.01	0.00
Na	0.02	0.05	0.10	0.09	0.15	0.10	0.12	0.09	0.19	0.11	0.15	0.09	0.05	0.13	0.12
K	0.00	0.00	0.00	0.00	0.01	0.01	0.00	0.00	0.01	0.00	0.01	0.00	0.00	0.00	0.00
Total	4.52	5.01	5.01	5.00	5.00	5.00	5.00	5.00	5.01	5.00	5.01	5.00	4.99	5.00	5.01
An	95.8	94.7	89.9	90.8	85.1	89.5	88.1	91.0	80.3	89.0	84.8	90.7	95.0	86.3	88.2
Ab	3.76	5.18	9.83	8.79	14.3	9.94	11.5	8.68	18.7	10.7	14.4	8.88	4.84	13.3	11.5
Or	0.40	0.10	0.29	0.40	0.69	0.60	0.39	0.30	1.08	0.30	0.79	0.39	0.20	0.40	0.30

	LEW 88009	LEW 88010	MAC 02522	MET 01081	Moama	Moore County	PCA 82501	PCA 91078	QUE 94484	QUE 97014	QUE 97053	QUE 99658	RKP A80224	Serra de Mage
SiO2	47.2	47.3	46.4	45.2	44.7	45.7	48.5	48.0	47.6	45.5	47.2	46.2	46.3	44.9
Al2O3	32.9	31.9	33.4	34.5	34.5	33.9	32.3	32.3	32.2	34.4	32.9	33.9	34.1	35.1
MgO	<0.03	<0.03	n.m.	<0.03	0.05	0.05	0.04	0.06	<0.03	<0.03	<0.03	<0.03	<0.03	0.04
CaO	16.9	16.7	17.9	18.3	19.4	18.6	16.0	16.9	17.3	18.2	16.9	17.1	18.0	19.3
FeO	0.45	0.45	0.24	0.19	0.11	0.07	0.25	0.23	0.43	0.11	0.20	0.15	0.06	0.06
Na2O	1.77	1.99	1.21	1.04	0.63	0.96	2.04	1.83	1.61	1.13	1.69	1.61	1.32	0.61
K2O	0.13	0.08	0.04	0.04	0.02	0.05	0.48	0.15	0.14	0.09	0.14	0.10	0.06	0.02
Total	99.28	98.37	99.08	99.33	99.41	99.42	99.70	99.48	99.28	99.48	99.03	99.02	99.79	100.00
Si	2.18	2.21	2.15	2.10	2.08	2.12	2.23	2.21	2.21	2.11	2.19	2.14	2.14	2.07
Al	1.80	1.76	1.83	1.89	1.89	1.85	1.75	1.76	1.76	1.88	1.80	1.86	1.85	1.91
Mg	0.00	0.00	n.m.	0.00	0.00	0.00	0.00	0.00	0.00	0.00	0.00	0.00	0.00	0.00
Ca	0.84	0.84	0.89	0.91	0.97	0.93	0.79	0.84	0.86	0.90	0.84	0.85	0.89	0.96
Fe	0.02	0.02	0.01	0.01	0.00	0.00	0.01	0.01	0.02	0.00	0.01	0.01	0.00	0.00
Na	0.16	0.18	0.11	0.09	0.06	0.09	0.18	0.16	0.15	0.10	0.15	0.15	0.12	0.05
K	0.01	0.01	0.00	0.00	0.00	0.00	0.03	0.01	0.01	0.01	0.01	0.01	0.00	0.00
Total	5.00	5.00	4.99	5.00	5.00	5.00	5.00	4.99	4.99	5.00	4.99	5.01	5.00	5.00
Ab	83.4	81.9	88.8	90.5	94.3	91.2	79.0	82.9	84.9	89.4	84.0	84.9	88.0	94.6
An	15.8	17.6	10.9	9.24	5.57	8.47	18.2	16.2	14.4	10.1	15.2	14.5	11.7	5.34
Or	0.80	0.49	0.30	0.30	0.10	0.30	2.80	0.89	0.79	0.49	0.80	0.60	0.30	0.10

Table 5: Representative analyses for metal and sulfides.

	ALH A81313		BTN 00300		Caldera	Chervony Kut	EET 87520	EET 90020		EET 90029	EET 92004	EET 92023			GRO 95533		Ibitira	LEW 85305
	Metal	Sulfide	Metal	Sulfide	Sulfide	Sulfide	Sulfide	Metal	Sulfide	Sulfide	Sulfide	Metal	Ni-rich Metal	Sulfide	Metal	Sulfide	Metal	Metal
Fe	100.1	63.8	100.2	63.0	64.0	62.7	62.1	100.2	63.9	63.8	62.9	95.2	51.9	63.7	99.6	63.7	99.1	99.8
Si	<0.03	<0.03	<0.03	0.03	<0.03	0.17	<0.03	<0.03	<0.03	<0.03	<0.03	<0.03	<0.03	<0.03	<0.03	<0.03	<0.03	0.04
Ni	0.49	<0.03	0.04	0.03	<0.03	<0.03	<0.03	0.20	<0.03	<0.03	0.07	5.15	48.31	0.10	0.43	0.05	1.06	0.25
Co	0.26	0.08	0.37	0.36	<0.03	<0.03	<0.03	<0.03	<0.03	<0.03	<0.03	1.37	0.25	<0.03	0.04	<0.03	0.49	0.09
S	<0.03	35.8	<0.03	35.5	35.5	35.9	34.2	<0.03	<0.03	35.9	36.0	<0.03	<0.03	36.3	<0.03	<0.03	<0.03	<0.03
P	<0.03	<0.03	<0.03	<0.03	<0.03	<0.03	<0.03	<0.03	35.2	<0.03	<0.03	<0.03	<0.03	<0.03	<0.03	35.5	<0.03	<0.03
Total	100.93	99.67	100.72	99.00	99.47	98.71	96.39	100.48	99.10	99.71	99.03	101.79	100.48	100.13	100.04	99.23	100.66	100.16
Fe	99.2	50.6	99.5	50.3	50.9	49.9	51.0	99.8	51.0	50.5	50.0	93.8	52.9	50.2	99.5	50.7	98.5	99.6
Si	0.04	0.00	0.04	0.04	0.02	0.26	0.01	0.00	0.00	0.01	0.00	0.03	0.02	0.01	0.02	0.03	0.01	0.07
Ni	0.46	0.00	0.04	0.03	0.00	0.00	0.00	0.19	0.00	0.00	0.05	4.83	46.83	0.07	0.40	0.03	1.00	0.24
Co	0.25	0.06	0.35	0.27	0.00	0.01	0.00	0.02	0.00	0.02	0.00	1.28	0.24	0.00	0.03	0.00	0.46	0.08
S	0.02	49.4	0.06	49.4	49.1	49.8	49.0	0.00	0.00	49.5	49.9	0.02	0.00	49.7	0.00	0.01	0.04	0.00
P	0.00	0.02	0.01	0.03	0.00	0.00	0.00	0.02	48.97	0.00	0.02	0.00	0.00	0.00	0.00	49.25	0.00	0.00
Total	100.00	100.00	100.00	100.00	100.00	100.00	100.00	100.00	100.00	100.00	100.00	100.00	100.00	100.00	100.00	100.00	100.00	100.00

	LEW 85353	LEW 88009	LEW 88010	MET 01081		Moama	Moore County		PCA 82501		PCA 91078	QUE 94484	QUE 97014		QUE 99658	RKP A80224	Serra de Mage
	Sulfide	Sulfide	Sulfide	Metal	Sulfide	Sulfide	Metal	Sulfide	Metal	Sulfide	Sulfide	Sulfide	Metal	Sulfide	Sulfide	Sulfide	Sulfide
Fe	63.1	63.2	62.9	100.2	63.0	99.2	100.1	63.3	100.7	63.6	62.4	63.4	100.3	63.4	62.0	63.0	63.7
Si	<0.03	0.09	0.04	<0.03	<0.03	0.11	<0.03	<0.03	<0.03	<0.03	<0.03	<0.03	<0.03	<0.03	0.11	<0.03	<0.03
Ni	0.03	<0.03	0.04	<0.03	<0.03	0.15	0.05	0.06	<0.03	<0.03	<0.03	<0.03	<0.03	<0.03	0.11	<0.03	<0.03
Co	<0.03	<0.03	0.13	0.42	0.02	0.16	0.42	<0.03	0.04	<0.03	<0.03	<0.03	0.15	0.04	0.24	0.45	0.04
S	35.2	35.7	36.2	0.03	36.0	<0.03	<0.03	35.7	<0.03	34.7	35.9	35.1	<0.03	34.3	35.8	36.3	34.8
P	<0.03	<0.03	<0.03	<0.03	<0.03	<0.03	<0.03	<0.03	<0.03	<0.03	<0.03	<0.03	<0.03	<0.03	<0.03	<0.03	<0.03
Total	98.29	99.01	99.28	100.64	99.06	99.64	100.56	99.03	100.78	98.34	98.36	98.52	100.46	97.68	98.25	99.71	98.58
Fe	50.7	50.3	49.9	99.5	50.1	99.5	99.5	50.5	99.9	51.3	49.9	50.9	99.8	51.5	49.7	49.7	51.2
Si	0.00	0.14	0.06	0.00	0.01	0.22	0.01	0.00	0.00	0.03	0.01	0.04	0.03	0.01	0.18	0.03	0.02
Ni	0.02	0.00	0.03	0.00	0.00	0.14	0.05	0.04	0.00	0.02	0.00	0.00	0.01	0.00	0.08	0.02	0.00
Co	0.01	0.00	0.10	0.39	0.02	0.15	0.40	0.00	0.03	0.01	0.00	0.00	0.14	0.03	0.18	0.34	0.03
S	49.3	49.5	49.9	0.04	49.8	0.0	0.0	49.5	0.02	48.7	50.1	49.1	0.0	48.5	49.9	49.9	48.8
P	0.01	0.00	0.01	0.03	0.01	0.00	0.02	0.00	0.00	0.01	0.03	0.00	0.00	0.00	0.00	0.00	0.00
Total	100.00	100.00	100.00	100.00	100.00	100.00	100.00	100.00	100.00	100.00	100.00	100.00	100.00	100.00	100.00	100.00	100.00

Table 6: Representative analyses for ilmenite.

	BTN 00300	Caldera	Chervony Kut	EET 87520	EET 90020	EET 90029	EET 92004	EET 92023	GRA 98098	GRO 95533	Ibitira	LEW 85305
SiO2	<0.03	0.03	<0.03	<0.03	<0.03	<0.03	<0.03	<0.03	<0.03	<0.03	0.04	<0.03
TiO2	52.9	52.4	52.8	52.6	53.2	52.7	52.2	52.3	52.7	52.4	52.3	52.2
ZrO2	<0.03	<0.03	<0.03	<0.03	0.05	<0.03	<0.03	<0.03	0.09	<0.03	0.12	0.04
Al2O3	<0.03	<0.03	<0.03	0.04	<0.03	<0.03	<0.03	<0.03	<0.03	<0.03	0.03	<0.03
Cr2O3	0.15	0.61	0.09	0.37	0.11	0.08	0.11	0.43	0.09	0.03	0.34	0.42
MgO	1.36	1.33	0.47	1.38	0.75	0.93	0.60	1.03	0.77	0.58	0.86	1.05
CaO	0.03	0.06	<0.036	0.16	<0.039	0.04	0.03	<0.03	<0.03	<0.031	0.07	0.06
MnO	0.80	0.81	0.96	0.81	0.72	0.90	0.93	1.04	0.71	0.97	0.59	0.79
FeO	44.3	44.0	44.7	43.8	44.3	45.4	45.5	44.5	45.1	45.2	44.8	44.4
Total	99.62	99.26	99.13	99.24	99.13	100.08	99.36	99.38	99.41	99.27	99.11	98.97
Si	0.00	0.00	0.00	0.00	0.00	0.00	0.00	0.00	0.00	0.00	0.00	0.00
Ti	1.00	0.99	1.01	1.00	1.01	1.00	1.00	0.99	1.00	1.00	1.00	0.99
Zr	0.00	0.00	0.00	0.00	0.00	0.00	0.00	0.00	0.00	0.00	0.00	0.00
Al	0.00	0.00	0.00	0.00	0.00	0.00	0.00	0.00	0.00	0.00	0.00	0.00
Cr	0.01	0.01	0.00	0.01	0.00	0.00	0.00	0.01	0.00	0.00	0.01	0.01
Mg	0.05	0.05	0.02	0.05	0.03	0.04	0.02	0.04	0.03	0.02	0.03	0.04
Ca	0.00	0.00	0.00	0.00	0.00	0.00	0.00	0.00	0.00	0.00	0.00	0.00
Mn	0.02	0.02	0.02	0.02	0.02	0.02	0.02	0.02	0.02	0.02	0.01	0.02
Fe	0.93	0.93	0.95	0.92	0.93	0.95	0.96	0.94	0.95	0.96	0.95	0.94
Total	2.00	2.00	1.99	2.00	1.99	2.00	2.00	2.00	2.00	2.00	2.00	2.00

	LEW 85353	LEW 88010	MET 01081	Moore County	PCA 82501	PCA 91078	PCA 91081	QUE 94484	QUE 97014	QUE 97053	QUE 99658	RKP A80224	Serra de Mage
SiO2	<0.03	<0.03	0.04	0.00	0.04	<0.03	<0.03	<0.03	<0.03	<0.03	0.04	<0.03	<0.03
TiO2	52.7	52.9	51.0	52.2	53.1	52.8	52.3	52.7	52.2	53.2	52.8	52.2	51.5
ZrO2	<0.03	<0.03	<0.03	<0.03	<0.03	<0.03	<0.03	<0.03	<0.035	<0.03	<0.03	<0.03	<0.03
Al2O3	<0.03	<0.03	0.07	0.11	<0.03	0.04	<0.03	<0.03	<0.03	<0.03	<0.03	<0.03	0.08
Cr2O3	0.18	0.07	1.29	2.47	0.05	0.29	0.08	0.03	<0.03	0.18	0.18	0.06	1.93
MgO	0.85	0.68	0.40	2.32	0.79	1.14	0.60	0.82	0.55	0.98	0.51	0.57	1.92
CaO	<0.037	0.03	0.32	<0.03	0.06	0.00	0.15	<0.03	0.05	0.07	0.15	<0.03	<0.03
MnO	0.87	0.88	0.98	0.84	0.90	0.82	0.88	1.34	0.94	0.91	0.80	0.89	1.03
FeO	45.2	45.3	44.8	41.7	44.6	44.1	45.5	44.6	45.0	44.6	45.0	45.4	42.5
Total	99.82	99.83	98.91	99.60	99.54	99.18	99.55	99.54	98.75	99.97	99.47	99.17	98.98
Si	0.00	0.00	0.00	0.00	0.00	0.00	0.00	0.00	0.00	0.00	0.00	0.00	0.00
Ti	1.00	1.00	0.98	0.98	1.00	1.00	0.99	1.00	1.00	1.00	1.00	1.00	0.97
Zr	0.00	0.00	0.00	0.00	0.00	0.00	0.00	0.00	0.00	0.00	0.00	0.00	0.00
Al	0.00	0.00	0.00	0.00	0.00	0.00	0.00	0.00	0.00	0.00	0.00	0.00	0.00
Cr	0.00	0.00	0.03	0.05	0.00	0.01	0.00	0.00	0.00	0.00	0.01	0.00	0.04
Mg	0.03	0.03	0.02	0.09	0.03	0.04	0.02	0.03	0.02	0.04	0.02	0.02	0.07
Ca	0.00	0.00	0.01	0.00	0.00	0.00	0.00	0.00	0.00	0.00	0.00	0.00	0.00
Mn	0.02	0.02	0.02	0.02	0.02	0.02	0.02	0.03	0.02	0.02	0.02	0.02	0.02
Fe	0.95	0.95	0.95	0.87	0.94	0.93	0.96	0.94	0.96	0.93	0.95	0.96	0.89
Total	2.00	2.00	2.01	2.00	1.99	2.00	2.01	2.00	2.00	2.00	2.00	2.00	2.00

Table 7: Representative analyses for ulvöspinel.

	ALH A81001	ALH A81313	BTN 00300	Caldera	Chervony Kut	EET 87520	EET 90020	EET 90029	EET 92004	EET 92023	GRA 98098	GRO 95533	Ibitira
SiO2	0.86	0.12	<0.03	<0.03	<0.03	<0.03	0.03	<0.03	0.07	0.05	<0.03	<0.03	<0.03
TiO2	2.15	2.98	12.2	15.3	12.1	12.1	16.7	5.67	3.60	5.35	21.7	7.58	12.0
ZrO2	<0.03	<0.03	<0.03	<0.03	<0.03	<0.03	<0.03	<0.03	<0.03	<0.03	<0.03	<0.03	<0.03
Al2O3	9.66	9.43	5.49	4.55	5.49	5.36	5.44	7.73	8.24	10.91	4.15	7.20	7.11
V2O3	0.64	0.64	0.81	0.81	0.58	0.56	0.58	0.83	0.89	0.43	0.51	0.56	0.63
Cr2O3	49.9	52.2	37.3	33.0	37.8	38.1	28.0	47.3	49.5	43.7	<0.03	44.2	35.3
MgO	0.36	2.34	1.01	0.98	1.08	1.08	0.43	0.72	0.46	1.25	0.69	0.69	0.70
CaO	0.20	<0.03	<0.03	<0.03	0.04	0.06	<0.03	0.06	0.03	0.14	<0.03	<0.03	0.04
MnO	0.57	0.56	0.59	0.55	0.47	0.52	0.61	0.47	0.52	0.53	0.55	0.59	0.48
FeO	33.9	32.1	42.0	44.6	41.5	41.5	47.4	36.5	35.4	35.9	51.5	38.2	42.8
Total	98.24	100.39	99.42	99.79	99.01	99.29	99.16	99.29	98.74	98.29	99.07	99.04	99.10
Si	0.03	0.00	0.00	0.00	0.00	0.00	0.00	0.00	0.00	0.00	0.00	0.00	0.00
Ti	0.06	0.08	0.33	0.42	0.33	0.33	0.46	0.15	0.10	0.14	0.60	0.21	0.33
Zr	0.00	0.00	0.00	0.00	0.00	0.00	0.00	0.00	0.00	0.00	0.00	0.00	0.00
Al	0.41	0.39	0.24	0.20	0.24	0.23	0.24	0.33	0.35	0.46	0.18	0.31	0.31
V	0.00	0.00	0.00	0.00	0.02	0.02	0.00	0.00	0.00	0.00	0.00	0.00	0.00
Cr	1.42	1.45	1.08	0.95	1.08	1.09	0.81	1.36	1.43	1.24	0.58	1.27	1.02
Mg	0.02	0.12	0.06	0.05	0.06	0.06	0.02	0.04	0.03	0.07	0.04	0.04	0.04
Ca	0.01	0.00	0.00	0.00	0.00	0.00	0.00	0.00	0.00	0.01	0.00	0.00	0.00
Mn	0.02	0.02	0.02	0.02	0.01	0.02	0.02	0.01	0.02	0.02	0.02	0.02	0.01
Fe	1.02	0.94	1.28	1.36	1.26	1.26	1.46	1.11	1.08	1.07	1.59	1.16	1.30
Total	2.99	3.00	3.01	3.00	3.00	3.00	3.01	3.00	3.01	3.01	3.01	3.00	3.01

	LEW 85305	LEW 85353	LEW 88009	LEW 88010	MAC 02522	MET 01081	Moama	Moore County	PCA 91078	QUE 97014	QUE 99658	RKP A80224	Serra de Mage
SiO2	<0.03	<0.03	<0.03	<0.03	1.08	0.04	<0.03	<0.03	<0.03	<0.03	0.06	<0.03	<0.03
TiO2	17.0	2.59	13.0	2.51	22.6	6.93	5.25	11.1	2.80	2.93	2.14	3.37	3.19
ZrO2	<0.03	<0.03	<0.03	<0.03	<0.03	<0.03	<0.03	<0.03	<0.03	<0.03	<0.03	<0.03	<0.03
Al2O3	4.21	8.46	4.32	8.54	3.51	7.89	7.59	5.89	11.64	8.14	12.87	8.12	8.43
V2O3	0.61	0.75	0.89	0.67	0.43	1.12	0.80	0.85	0.00	0.95	0.56	0.93	0.63
Cr2O3	29.4	53.0	37.9	53.5	17.9	43.1	49.5	39.8	47.9	51.1	48.8	51.0	51.4
MgO	0.71	0.60	0.45	0.38	0.99	0.35	2.42	1.87	1.00	0.50	0.83	0.43	1.87
CaO	<0.03	<0.03	0.12	<0.03	0.13	0.08	<0.03	0.00	<0.03	0.12	0.11	0.05	<0.03
MnO	0.50	0.45	0.60	0.47	0.58	0.59	0.63	0.53	0.55	0.58	0.50	0.57	0.58
FeO	46.8	33.8	43.1	33.9	51.6	38.6	33.1	39.0	34.5	34.3	34.2	35.1	32.3
Total	99.15	99.65	100.40	100.01	98.89	98.73	99.21	99.14	98.41	98.66	100.05	99.55	98.42
Si	0.00	0.00	0.00	0.00	0.04	0.00	0.00	0.00	0.00	0.00	0.00	0.00	0.00
Ti	0.47	0.07	0.36	0.07	0.62	0.19	0.14	0.30	0.08	0.08	0.06	0.09	0.09
Zr	0.00	0.00	0.00	0.00	0.00	0.00	0.00	0.00	0.00	0.00	0.00	0.00	0.00
Al	0.18	0.36	0.19	0.36	0.15	0.34	0.32	0.25	0.49	0.35	0.53	0.35	0.36
V	0.00	0.00	0.00	0.00	0.00	0.03	0.00	0.00	0.00	0.00	0.00	0.00	0.00
Cr	0.86	1.51	1.09	1.52	0.52	1.24	1.40	1.14	1.35	1.48	1.35	1.46	1.46
Mg	0.04	0.03	0.02	0.02	0.05	0.02	0.13	0.10	0.05	0.03	0.04	0.02	0.10
Ca	0.00	0.00	0.00	0.00	0.01	0.00	0.00	0.00	0.00	0.00	0.00	0.00	0.00
Mn	0.02	0.01	0.02	0.01	0.02	0.02	0.02	0.02	0.02	0.02	0.01	0.02	0.02
Fe	1.44	1.02	1.32	1.01	1.59	1.17	0.99	1.18	1.03	1.05	1.00	1.06	0.97
Total	3.01	3.00	3.00	2.99	3.00	3.01	3.00	3.00	3.01	3.01	3.00	3.00	3.00

Table 8: The opaque minerals present within the unbrecciated eucrites[a].

Group	Samples	Chr/Usp	Ilmenite	Sulphide	Metal
Basaltic	ALH A81001	N	Y[b]	N	N
	ALH A81313	Y	N	Y	Y
	BTN 00300	Y	Y	Y	Y
	Caldera	Y	Y	Y	N
	Chervony Kut	N	Y	Y	N
	EET 87520	Y	Y	Y	N
	EET 90020	Y	Y	Y	Y
	EET 90029	Y	Y	Y	N
	EET 92004	Y	Y	Y	N
	EET 92023	Y	Y	Y	Y
	GRA 98098	Y	Y	N	N
	GRO 95533	Y	Y	Y	Y
	Ibitira	Y	Y	N	Y
	LEW 85305	Y	Y	N	Y
	LEW 85353	Y	Y	Y	N
	LEW 88009	Y	N	Y	N
	LEW 88010	Y	Y	Y	N
	MAC 02522	Y	N	N	N
	MET 01081	Y	Y	Y	Y
	PCA 82501	N	Y	Y	Y
	PCA 91007	Y	Y	N	N
	PCA 91078	Y	Y	Y	N
	PCA 91081	Y	N	N	N
	QUE 94484	Y[c]	Y	Y	N
	QUE 97014	Y	Y	Y	Y
	QUE 97053	Y	Y	N	N
	QUE 99658	Y	Y	Y	N
	RKP A80224	Y	Y	Y	N
Cumulate	Moama	Y	N	N	Y
	Moore County	Y	Y	Y	Y
	Serra de Mage	Y	Y	Y	N

[a]Y indicates that mineral is present and analyzed. N indicates that it was not observed in that sample, Chr/Usp = Chromite/Ulvöspinel

[b] This mineral was analyzed but good totals could not be achieved due to grain size.

[c] This minerals was analyzed but good totals could not be achieved due to oxidation.

Table 9: Degree of metamorphic equilibration in the unbrecciated eucrites[a].

Sample	Group	Exsolution T °C		Pyx Major	Pyx Minor	Plag <5%An	Total
EET 90020	Granoblastic	1095	±75	Y	Y	Y	3
Caldera	Basaltic	1034	±88	Y	Y	Y	3
BTN 00300	Granoblastic	1024	±74	Y	Y	Y	3
PCA 91078	Basaltic	1012	±68	Y	N	N	1
EET 87520	Basaltic	1010	±94	Y	Y	Y	3
GRA 98098	Granoblastic	985	±78	Y	Y	N	2
Ibitira	Granoblastic	979	±54	Y	Y	Y	3
Moore County	Cumulate	934	±54	Y	Y	Y	3
MET 01081	Basaltic	919	±72	Y	Y	Y	3
Moama	Cumulate	906	±33	Y	Y	Y	2
ALH A81313	Basaltic	891	±29	Y	Y	Y	2
PCA 91007	Basaltic	872	±28	Y	N	N	2
LEW 85305	Granoblastic	834	±39	Y	Y	N	2
EET 90029	Basaltic	817	±32	Y	N	Y	2
QUE 97053	Basaltic	801	±24	Y	N	N	1
PCA 91081	Basaltic	800	±10	Y	N	N	1
Serra De Mage	Cumulate	794	±24	Y	Y	Y	3
PCA 82501	Basaltic	784	±36	Y	N	N	1
EET 92004	Basaltic	738	±39	Y	N	N	1
GRO 95533	Basaltic	706	±30	Y	N[a]	N	1
RKP A80224	Basaltic	698	±21	Y	N	Y	2
LEW 85353	Basaltic	692	±17	Y	N	Y	2
Chervony Kut	Basaltic	685	±32	Y	N	Y	2
PCA 97014	Basaltic	685	±7	Y	N	Y	2
ALH A81001	Basaltic	680	±23	Y	N	N/A	1[b]
QUE 99658	Basaltic	677	±31	Y	N	N	1
LEW 88009	Basaltic	654	±29	Y	N	N	1
LEW 88010	Basaltic	654	±46	Y	N	N	1
QUE 94484	Basaltic	N/A		N	N[a]	N	0
MAC 02522	Basaltic	N/A		N	N	N	0

[a]Y denotes sample is equilibrated with respect to that component, N denotes that it is not.
[b]These components are very close to being judged as equilibrated.